

XMM-Newton Observation of an X-ray Trail Between the Spiral Galaxy NGC 6872 and the Central Elliptical NGC 6876 in the Pavo Group

Marie E. Machacek, Paul Nulsen, Liviu Stirbat, Christine Jones, and William R. Forman

*Harvard-Smithsonian Center for Astrophysics, MS67,
60 Garden Street, Cambridge, MA 02138 USA*

`mmachacek@cfa.harvard.edu`, `pnulsen@head-cfa.cfa.harvard.edu`,
`lstirbat@fas.harvard.edu`, `cjf@head-cfa.cfa.harvard.edu`,
`wrf@head-cfa.cfa.harvard.edu`

ABSTRACT

We present XMM-Newton observations of a trail of enhanced X-ray emission extending along the full $8'.7 \times 4'$ region between the large spiral galaxy NGC 6872 and the dominant elliptical galaxy NGC 6876 in the Pavo Group, the first known X-ray trail associated with a spiral galaxy in a poor galaxy group and, with projected length of 90 kpc, one of the longest X-ray trails observed in any system. The X-ray surface brightness in the trail region is roughly constant beyond ~ 20 kpc of NGC 6876 in the direction of the spiral. The trail is hotter (~ 1 keV) than the undisturbed Pavo IGM (~ 0.5 keV) and has low metal abundances ($0.2 Z_{\odot}$). The $0.5 - 2$ keV luminosity of the trail, measured using a 67×90 kpc rectangular region, is 6.6×10^{40} erg s $^{-1}$. We compare the properties of gas in the trail to the spectral properties of gas in the spiral NGC 6872 and in the elliptical NGC 6876 to constrain its origin. We suggest that the X-ray trail is either IGM gas gravitationally focused into a Bondi-Hoyle wake, a thermal mixture of $\sim 64\%$ Pavo IGM gas with $\sim 36\%$ galaxy gas that has been removed from the spiral NGC 6872 by turbulent viscous stripping, or both, due to the spiral's supersonic motion at angle $\xi \sim 40^\circ$ with respect to the plane of the sky, past the Pavo group center (NGC 6876) through the densest region of the Pavo IGM. Assuming $\xi = 40^\circ$ and a filling factor η in a cylindrical volume with radius 33 kpc and projected length 90 kpc, the mean electron density and total hot gas mass in the trail is $9.5 \times 10^{-4} \eta^{-1/2}$ cm $^{-3}$ and $1.1 \times 10^{10} \eta^{1/2} M_{\odot}$, respectively.

Subject headings: galaxies: clusters: general — galaxies: individual (NGC 6876, NGC 6872) — intergalactic medium — X-rays: galaxies

1. Introduction

The study of galaxy interactions with each other and with intragroup gas in nearby galaxy groups provides a template for understanding galaxy evolution at high redshift, a time when, according to hierarchical models, galaxies were rapidly coalescing through accretion and merger into groups and clusters, enriching, if not producing, the intragroup medium (IGM), and evolving into their present day morphological mix. Physical processes expected to be important for this evolution form two broad classes: (1) tidal interactions such as those induced by major mergers (Lavery & Henry 1988), off-axis galaxy collisions (Müller et al. 1989), galaxy harassment (Moore et al. 1996) or galaxy fly-bys near the core of the group/cluster potential (Byrd & Valtonen 1990), and (2) gas-gas interactions, notably ram pressure by the intracluster (ICM) or group IGM gas on the galaxy’s interstellar medium (ISM), due to the galaxy’s motion through the surrounding medium (Gunn & Gott 1972), or ISM-ISM interactions produced in galaxy-galaxy collisions (Kenney et al. 1995). These gas-dynamical processes may be enhanced by turbulence and viscous effects (Nulsen 1982; Quilis et al. 2000) or inhomogeneities and bulk motions in the ICM/IGM gas (Kenney et al. 2004). The actions of tidal forces are identified by the appearance of disturbed stellar morphologies, such as stretched stellar tails and folds (see e.g. Gnedin 2003, Vollmer 2003). Observations and simulations suggest that minor mergers and off-axis collisions often induce non-axisymmetric tidal distortions in the central regions of the interacting galaxies, initiating gas inflow and starbursts (Kannappan et al. 2004) or other nuclear activity. These may cause superwinds and outflow bubbles, identifiable by their X-ray signatures (Cecil et al. 2002; Strickland et al. 2004).

Key observational signatures for ram pressure stripping by the ICM/IGM are the appearance of “cold fronts” (e.g. Vikhlinin et al. 2001; Heinz et al. 2003) and X-ray wakes or tails (Stevens et al. 1999; Schulz & Struck 2001; Acreman et al. 2003). While these features have been studied in a number of nearby galaxies, primarily ellipticals in rich cluster environments, e.g. NGC 1404 (Jones et al. 1997; Paolillo et al. 2002; Machacek et al. 2004; Scharf et al. 2004) in Fornax and M86 (Forman et al. 1979; White et al. 1991; Rangarajan et al. 1995) and NGC 4472 (Irwin & Sarazin 1996; Biller et al. 2004) in Virgo, wakes and tails are low surface brightness structures whose observation is still relatively rare. In hot clusters this is due in part to the rapid depletion of galactic gas by the dense ICM near the cluster cores, and also to the difficulty of observing a low surface brightness feature against the bright cluster background (Acreman et al. 2003). Galaxy groups possess a significant, albeit cooler, gaseous IGM component (Mulchaey et al. 1996, 2003; Ponman et al. 1996; Osmond & Ponman 2004). Thus gas-gas interactions can occur, with the resulting wakes and debris trails perhaps easier to study (Acreman et al. 2003; Stevens et al. 1999). Furthermore, investigation of these systems may illuminate the still controversial role of ram

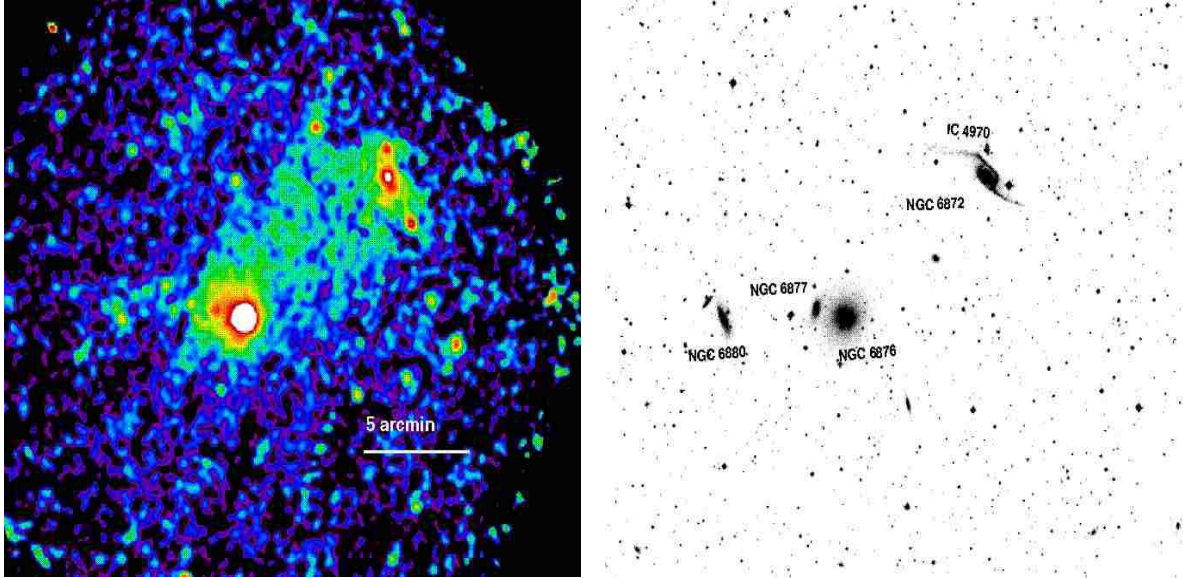


Fig. 1.— (left) The XMM-Newton 0.5 – 2 keV background-subtracted, exposure corrected, coadded MOS and PN images of the Pavo Group showing the X-ray trail of enhanced emission connecting, in projection, the spiral galaxy NGC 6872 (upper right) to the dominant elliptical NGC 6876 (lower left). The color scale has logarithmic stretch from 5×10^{-8} to 3×10^{-4} photons s $^{-1}$ arcsec $^{-2}$. The X-ray trail is evidence of NGC 6872’s interaction with the group. (right) The DSS image of the same field matched in WCS coordinates, with the five Pavo galaxies (NGC 6872, IC 4970, NGC 6876, NGC 6877, NGC 6880) that are also detected in X-rays labeled. Other galaxies in the field are IC 4981 to the northeast of NGC 6880, IC 4972 to the southwest of NGC 6876, and PCG 64439 midway, in projection, between NGC 6876 and NGC 6872.

pressure in either enhancing or quenching star formation within the affected galaxy (Fujita 1998; Kenney et al. 2004).

In this paper we present the XMM-Newton X-ray observation¹ of the X-ray trail extending between the dominant elliptical galaxy NGC 6876 and the large spiral galaxy NGC 6872 in the Pavo group. This is one of the few known X-ray trails associated with a large spiral galaxy (see Wang et al. 2004; Sun & Vikhlinin 2004) and the first such trail observed in a poor galaxy group. As shown in Figure 1, the Pavo group, LGG 432 in the Lyon Groups of Galaxies catalogue (Garcia 1993) with the addition of NGC 6872 and its companion IC 4970

¹Based on observations obtained with the XMM-Newton, an ESA science mission with instruments and contributions directly funded by ESA Member States and NASA

(Green et al. 1988), is a southern galaxy group comprised of ~ 11 galaxies. The $18' \times 18'$ Digitized Sky Survey (DSS) field (right panel) shows eight of these galaxies including the central, dominant elliptical galaxy NGC 6876 and the giant, spiral galaxy NGC 6872. In the left panel of Figure 1 we show $0.5 - 2$ keV coadded XMM-Newton MOS and PN images. Before being smoothed by a Gaussian with $\sigma = 7''.5$, the X-ray images were background subtracted and then corrected for telescope vignetting and the spatial dependence of the instrument response by use of exposure maps. The most striking feature in this image, other than emission from five individual galaxies, is the extensive trail of enhanced X-ray emission spanning nearly the full $8'.7 \times 4'$ (~ 130 kpc \times 60 kpc) projected area between the dominant elliptical NGC 6876 (near the center of the image) and the large spiral NGC 6872 (upper right). The image also suggests possible filamentary structure within the trail, with a reduction in flux by $\sim 28\%$ in the central region of the trail, near the line joining the two large galaxies.

Both large galaxies in the field, the dominant elliptical NGC 6876 and the spiral NGC 6872, have been observed previously in a variety of wavelength bands and show evidence for past or ongoing interactions within the Pavo group. The dominant group galaxy NGC 6876 ($\alpha = 20^h 18^m 19.15^s$, $\delta = -70^\circ 51' 31''.7$) has been observed in the optical, near-infrared (NIR), and mid-infrared (mid-IR) as well as in X-rays. Optical and NIR Hubble Space Telescope observations of the inner $5''$ of NGC 6876 show a flat core with depressed surface brightness at the center with no evidence for dust absorption (Lauer et al. 2002). This has been interpreted as evidence that a binary black hole resides within $0.''2$ of the center of the galaxy, a remnant of prior merging activity. As shown in Figure 1, a smaller elliptical galaxy NGC 6877 lies only $1'.4$ in projection to the east-northeast of NGC 6876. Since the relative radial velocity between NGC 6876 and NGC 6877 is small ($\Delta v_r \sim 296 \pm 44$ km s $^{-1}$, Martimbeau & Huchra 2004), the two galaxies might form an interacting pair. However, little evidence for any interaction has been found. In particular, the upper limit on H α emission in NGC 6876, $L_{\text{H}\alpha} < 2.7 \times 10^{39}$ erg s $^{-1}$ (Macchetto et al. 1996) indicates little ongoing star formation at the present time, that might be expected if the galaxies were interacting. NGC 6876 has been observed in X-rays by Einstein (Fabbiano et al. 1992; Burstein et al. 1997), ROSAT PSPC (O’Sullivan et al. 2001), ASCA (Buote & Fabian 1998; Davis et al. 1999) and XMM-Newton (this work). The left panel of Figure 1 shows X-ray emission from both NGC 6876 and NGC 6877, forming, in projection, an asymmetric extension to the east. Prior X-ray observations lacked the angular resolution to separate these two contributions, and it is still unclear whether the common envelope of X-ray emission is primarily a projection effect or evidence for interaction.

NGC 6872 ($\alpha = 20^h 16^m 56.48^s$, $\delta = -70^\circ 46' 5.7''$) is a bright, barred spiral galaxy in the Pavo group with long, thin, tidally-distorted stellar arms stretching $> 4'$ in extent (see Figure

1). It has been observed in X-rays by Einstein (Fabbiano et al. 1992; Burstein et al. 1997) as well as by XMM-Newton. $\text{H}\alpha$ emission, while absent from the central region of the galaxy, is found concentrated along the spiral arms (Mihos et al. 1993), consistent with recent star formation activity. Star formation is concentrated in regions of the highest measured $\text{H}\alpha$ velocity dispersions, suggesting that it is collisionally induced. From 21 cm observations, Horellou & Booth (1997) and Horellou & Koribalski (2003) showed that $\sim 1.82 \times 10^{10} M_\odot$ (for an assumed distance $D = 59.8 \text{ Mpc}$) of HI gas is distributed along and beyond the stellar arms, avoiding the central bulge and bar regions of the galaxy. The extension of HI along the northern arm of the galaxy has a “knee” roughly coincident with the location of a smaller companion galaxy IC 4970 located $1'.12$ in projection to the north of NGC 6872. A tidally disturbed stellar bridge between IC 4970 and NGC 6872, coupled with their small relative radial velocity $\Delta v_r = 74 \pm 62 \text{ km s}^{-1}$ (Martimbeau & Huchra 2004), indicates that the two galaxies are interacting. This led to the suggestion that an off-axis collision may be responsible for both the tidal distortions and star formation in the arms of NGC 6872 (Mihos et al. 1993; Horellou & Koribalski 2003). Simulations of a prograde, parabolic, low inclination collision of IC 4970 with NGC 6872 (Mihos et al. 1993) successfully reproduced NGC 6872’s stellar bar, the extent of the tidally distorted arms and tidal debris near IC 4970. However, the simulations required a mass-to-light ratio in IC 4970 twice that in NGC 6872. The simulations also failed to reproduce the thinness of the spiral arms, and did not explain why gas was distributed at large radii, thus preventing the collision from inducing star formation in the bar and nuclear regions. The elliptical NGC 6876 was not thought to contribute to the morphological distortion of NGC 6872 (Mihos et al. 1993) because of its ~ 8 times larger projected distance ($\sim 8'.7$) from the spiral galaxy and the significant relative radial velocity ($849 \pm 28 \text{ km s}^{-1}$, Martimbeau & Huchra 2004) between them. However, our present analysis using X-ray data from the XMM-Newton satellite shows a trail of enhanced X-ray emission, extending over nearly the full $8'.7 \times 4'$ region, between the dominant elliptical NGC 6876 and the large spiral NGC 6872. The extent of the X-ray trail, as well as the morphology of NGC 6872’s spiral arms, suggests that NGC 6872 interacted strongly with NGC 6876 and/or with the group gas during its passage through the Pavo group.

In Section 2 we detail the observation and the analysis procedures used. In Section 3 we present our main results. In Section 3.1 we use exposure-corrected X-ray images to compare the surface brightness profiles of the enhanced X-ray emission (the X-ray trail) between the dominant elliptical NGC 6876 and the large spiral NGC 6872 with those of the undisturbed Pavo IGM. In Section 3.2 we determine the spectral properties of the Pavo IGM, the X-ray trail, and the two dominant galaxies, NGC 6876 and NGC 6872, and, in Section 3.3, estimate their mean electron densities and mass contained in hot gas. In Section 4 we interpret these results arguing that the X-ray trail is most likely either gas removed from

NGC 6872 by turbulent viscous stripping (Nulsen 1982) and then thermally mixed with Pavo IGM gas, IGM gas gravitationally focused into a Bondi-Hoyle wake, or both. Each process is a result of the supersonic motion of the large spiral NGC 6872 past the group center (near NGC 6876) through the densest part of the Pavo IGM. We summarize our results in Section 5. Unless stated otherwise, all fluxes are observed fluxes, while all luminosities are intrinsic, i.e. corrected for absorption. All uncertainties are 90% confidence limits. Assuming that the distance to the Pavo group is well represented by the distance to the dominant elliptical NGC 6876 ($D = 53.5$ Mpc given $z = 0.01338$, from NED², and $H_0 = 75 \text{ km s}^{-1} \text{ Mpc}^{-1}$), 1" corresponds to a physical distance scale of 255 pc.

2. Observations and Analysis

Our observation consists of a 32.2 ks exposure of the Pavo group taken by the XMM-Newton satellite on 31 March - 1 April 2002. The data were obtained using the EPIC camera with MOS1, MOS2 and PN detectors active, operating in the full-frame mode with thin filter. The data were analyzed using the standard X-ray processing packages: SAS 5.4, CIAO 3.1, FTOOLS and XSPEC 11.2. The data were cleaned to keep only standard patterns ≤ 12 for MOS and ≤ 4 for PN. Bad pixels and columns also were removed in the standard manner. Periods of anomalously high background (flares) were identified and removed from the data using light curves for each detector in the 0.2 – 12 keV and 10 – 12 keV bandpasses, and in the 1 – 5 keV bandpass in an outer 11' – 12' annulus, where the effective area is small. This reduced the useful exposure times to 17.7 ks, 18.8 ks, and 10.6 ks for the MOS1, MOS2, and PN detectors, respectively.

Backgrounds were subtracted using source free background event files (Read & Ponman 2003) provided by the XMM-Newton Science Operations Center³ appropriate for the detector, mode and filter with effective exposure times of 1,055, 905 s, 1,004, 709 s, and 351, 549 s for the MOS1, MOS2, and PN detectors, respectively. The backgrounds were projected onto the coordinates of the current observation and identical spatial and energy filters were applied to source and background data throughout, so that the background normalization is set by the ratio of exposure times. This normalization was checked by comparing count rates between the Pavo observation and background files in both the high energy (10 – 12 keV) band and in an outer (11' – 12') annular ring at 1 – 5 keV, where background is expected to dominate. We found that the backgrounds differed by $\lesssim 6\%$ for MOS ($\lesssim 16\%$ for PN) in the

²<http://nedwww.ipac.caltech.edu/>

³see http://xmm.vilspa.esa.es/external/xmm_sw_cal/calib/epic_files.shtml

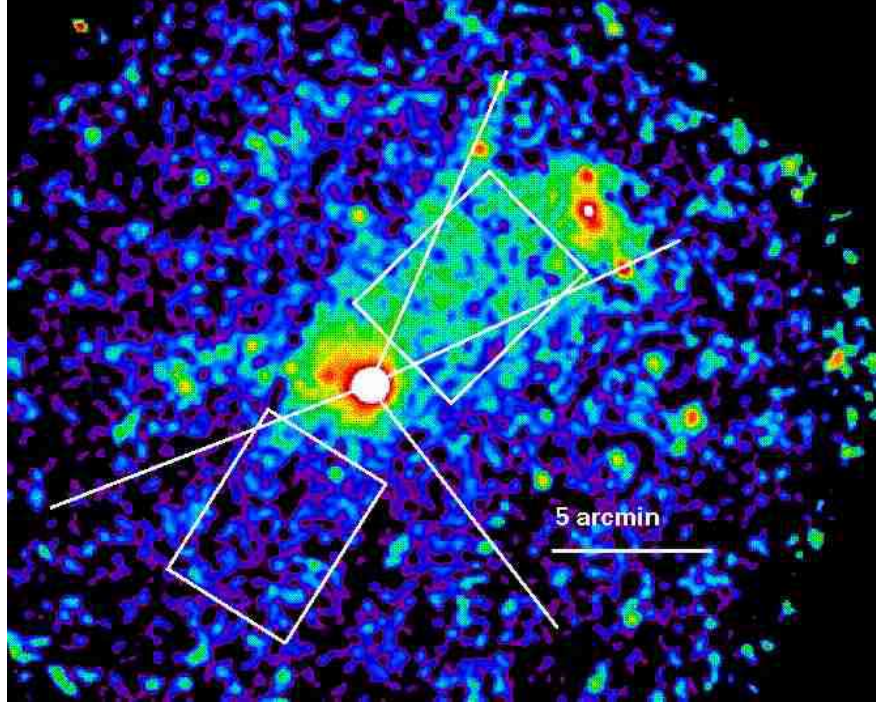


Fig. 2.— The same $0.5 - 2$ keV background-subtracted, exposure corrected, coadded XMM-Newton images of the Pavo group shown in Figure 1 overlaid with the regions used for analysis. North is up and east is to the left. Lines outline the northwestern and southern angular sectors used to measure the surface brightness profiles, shown in Figure 3, of the X-ray trail and Pavo IGM, respectively. Rectangular regions denote the spectral extraction regions for the X-ray trail (northwest) and the Pavo IGM (south).

10 – 12 keV band and $\lesssim 3\%$ for all detectors in the $1 - 5$ keV band for the outer annular ring. We adopt these values as measures of the remaining relative uncertainty in the background levels. Point sources were identified in the field shown in Figure 2, over the $0.5 - 10$ keV energy band, using a multiscale wavelet decomposition algorithm set with a 5σ detection threshold. Nineteen sources were identified, in addition to emission from five Pavo galaxies (NGC 6876, NGC 6877, NGC 6880, NGC 6872, and IC 4970) shown in Figure 1, and were excluded from our surface brightness and spectral analyses.

3. Results

Figure 2 presents the same $0.5 - 2$ keV coadded XMM-Newton images of the central $12'$ circular field of the Pavo Group shown in the left panel of Figure 1 with regions outlined for analysis. We construct surface brightness profiles for the MOS and PN detectors separately, because of their differing effective areas. We use the angular sectors, shown in Figure 2, centered on NGC 6876 extending from 23.6° to 65° to the northwest for the X-ray trail and from 142° to 249° to the south for the Pavo IGM. All angles are measured clockwise from north. We excluded pixels with anomalously low efficiency ($< 0.45\%$) in order to mitigate any possible artificial enhancement of low surface brightness fluctuations due to poor detector response. We also show in Figure 2 the $4'.35 \times 5'.9$ (67 kpc \times 90 kpc) rectangular spectral extraction regions, for the X-ray trail to the northwest and for the Pavo IGM to the south of NGC 6876. These two rectangular spectral extraction regions are at roughly equivalent off-axis distances in the detectors, so that the variation of the telescope effective area over the two regions is nearly the same.

3.1. The Surface Brightness Asymmetry

In Figure 3 we present the background-subtracted, $0.5 - 2$ keV surface brightness profiles for the X-ray trail (filled symbols) and for the Pavo IGM (open symbols) for data from the combined MOS detectors (circles) and from the PN detector (squares, after rescaling by the ratio of the MOS to PN detector effective areas in the $0.5 - 2$ keV band), measured in the angular sectors shown in Figure 2. For the southern sector, the surface brightness profile for NGC 6876, is well represented by the sum of two β -models, a central galactic (NGC 6876) or group core component with core radius $r_c = 5$ kpc ($20''$) and $\beta = 0.65$ and an extended IGM component with core radius $r_c = 50$ kpc ($196''$) and $\beta = 0.3$, out to a radius of $r \sim 120$ kpc ($\sim 8'$). Such a two component β -model characterization of the surface brightness profile is expected for galaxy groups containing significant amounts of group IGM gas (Mulchaey & Zabludoff 1998). The values we find for the core radii and β indices are in good agreement with those found in recent surveys of the X-ray emission from similar systems that show extended X-ray gas and a dominant elliptical at the group center (Mulchaey et al. 2003; Osmond & Ponman 2004).

The surface brightness profile in the northwest angular sector is clearly different from the southern sector. Within 20 kpc the profile is well described by the galactic component ($r_c = 5$ kpc, $\beta = 0.65$) alone, while beyond 20 kpc (in the X-ray trail) the surface brightness is constant or slowly rising. For projected distances $\gtrsim 60$ kpc from the center of the dominant elliptical NGC 6876, the $0.5 - 2$ keV surface brightness in the northwest region containing

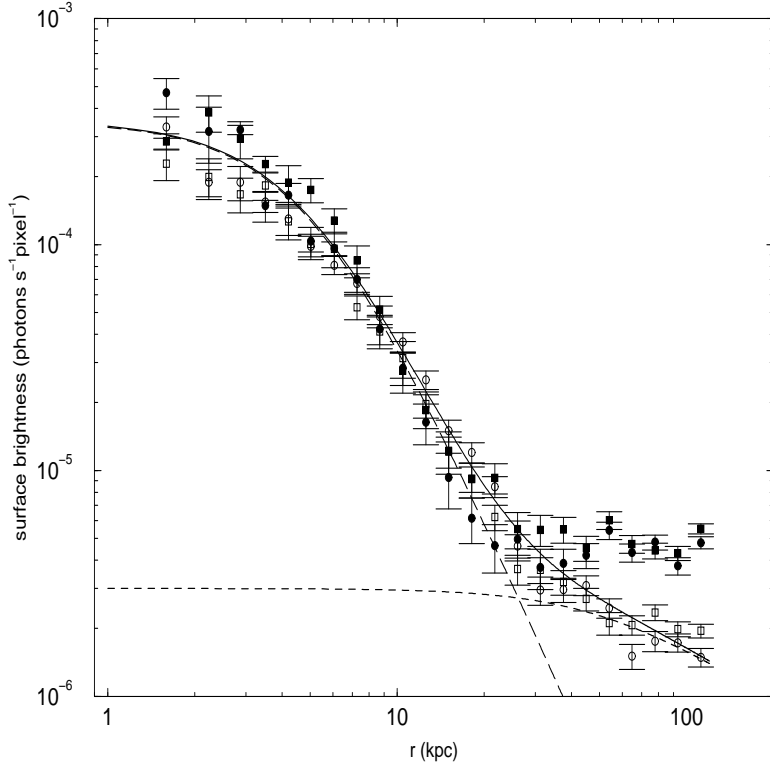


Fig. 3.— Background-subtracted surface brightness profiles for 0.5 – 2 keV X-ray emission from the elliptical galaxy NGC 6876 through the X-ray trail towards the spiral NGC 6872 (filled symbols) and from NGC 6876 through the undisturbed Pavo IGM to the south (open symbols) using the angular sectors shown in Figure 2. Circles denote the combined MOS1 and MOS2 data. Squares denote the PN data rescaled by the ratio of the effective areas of the MOS and PN detectors. Lines denote the β -models used to describe the data: a galactic component for NGC 6876 with core radius $r_c = 5$ kpc and $\beta = 0.65$ (long-dashed line), a Pavo IGM component with $r_c = 50$ kpc and $\beta = 0.3$ (short dashed line), and the sum of the galactic and IGM components (solid line).

the X-ray trail is a factor $\gtrsim 2$ larger than that of the undisturbed Pavo IGM at the same projected distance to the south.

3.2. Spectral Properties

To investigate the origin of the enhanced emission in the X-ray trail between the elliptical galaxy NGC 6876 and the spiral galaxy NGC 6872, we need to compare the temperature,

metal abundances and density of gas in the X-ray trail to that in the undisturbed Pavo IGM and in the galaxies, NGC 6876 and NGC 6872, that lie at either end of the X-ray trail. We extract spectra from circular regions surrounding the two large galaxies in addition to the spectra from the rectangular regions (shown in Figure 2) for the X-ray trail and Pavo IGM. For the spiral NGC 6872, we use a $58''.6$ (14.9 kpc) circular region about the center of the galaxy to maximize the count rate, while keeping the region as homogeneous as possible. This region includes the bulge of the galaxy and inner portions of the northern and southern spiral arms (see Figure 1), but excludes the interacting companion galaxy IC 4970 and extended tidal distortions. For the dominant elliptical galaxy NGC 6876, we consider two regions, a $62''.7$ (16 kpc) circular region (denoted NGC 6876 main) for the central emission from the galaxy, and a $99''.7$ (25.4 kpc) circular region (denoted NGC 6876 extended), to include the extended envelope of emission to the east-northeast, but with a $10''$ (2.6 kpc) circular region that excludes NGC 6877. For both the northwest region of enhanced emission and the southern undisturbed Pavo IGM, the X-ray emission is soft with count rates above 2 keV consistent with background. We restrict these spectral fits to the $0.5 - 2$ keV bandpass. Spectra for the galaxies may be harder due to either unresolved X-ray binaries or nuclear activity. Thus we consider the full $0.5 - 5$ keV bandpass for NGC 6876 and NGC 6872, where the MOS and PN detectors have good efficiency and the calibrations are well determined. For all spectra, counts are grouped using pre-defined groupings resulting

Table 1. Absorbed Apec Model Fits to the Pavo IGM and the X-ray Trail

Region/Model	MOS1, MOS2, PN source counts	kT keV	A Z_\odot	χ^2/dof
IGM	348, 366, 926	$0.50^{+0.06}_{-0.05}$	$0.05^{+0.03}_{-0.02}$	43.3/39
Trail 1T	788, 841, 2000	$0.66^{+0.07}_{-0.03}$	$0.06^{+0.01}_{-0.02}$	83.6/39
Trail 2T	788, 841, 2000	$0.98^{+0.06}_{-0.07}$	0.2 ± 0.1	54.0/39

Note. — Absorbed APEC model fits to the Pavo IGM and to the debris field between NGC 6876 and NGC 6872 with fixed Galactic absorption ($4.97 \times 10^{20} \text{ cm}^{-2}$). “Trail 1T” denotes a single temperature APEC model. “Trail 2T” denotes a two temperature APEC model with one set of parameters fixed at the IGM model best fit values given in row “IGM”; while those for the X-ray trail are free to vary. All fits use the $0.5 - 2.0$ keV bandpass.

in channels of approximately constant logarithmic width. The data from the MOS1, MOS2, and PN detectors, for a given extraction region, are fit simultaneously using XSPEC 11.2.

3.2.1. Spectral Properties of the Trail and Pavo IGM

We consider a variety of possible absorbed APEC plasma models to describe the spectra for gas in the X-ray trail and Pavo IGM. These results are summarized in Table 1. We are unable to allow all the model parameters to vary freely in these fits to the Pavo IGM gas in the southern region, due to the faintness of the emission. We fix the absorbing column at the Galactic value⁴ ($n_{\text{H}} = 4.97 \times 10^{20} \text{ cm}^{-2}$), because physically we would not expect excess absorption in the undisturbed group gas. Furthermore previous fits to ASCA data for the Pavo group (Davis et al. 1999) found an absorbing column consistent with Galactic. We find a temperature $kT = 0.50_{-0.05}^{+0.06} \text{ keV}$ and metal abundances $A = 0.05_{-0.02}^{+0.03} Z_{\odot}$ for the Pavo IGM gas in the southern rectangular region. The abundances are in good agreement with the results by Davis et al. (1999), who find, using ASCA data, $A = 0.09_{-0.06}^{+0.36}$; however, the temperature we find is a factor ~ 1.7 lower. As we will discuss below, their higher temperature for the Pavo group gas is due primarily to the inclusion of both the debris trail and the dominant elliptical galaxy NGC 6876 in their measurements. We show our fit to the Pavo IGM spectrum in the left panel of Figure 4.

As shown in the right panel of Figure 4, the spectrum for gas in the enhanced X-ray emission trail between NGC 6876 and NGC 6872 (northwestern rectangular region in Figure 2) is harder than that of the Pavo IGM to the south. A single temperature APEC model does not provide an acceptable fit to the data. The data are well described using a two component APEC model with one set of parameters (temperature, abundance, and normalization) fixed at the best Pavo IGM values from Table 1 to account for background emission from the Pavo IGM, while the temperature, abundance and normalization of the second component, modelling the gas in the X-ray trail, are allowed to vary. The absorbing column is again fixed at the Galactic value. The temperature of the gas in the X-ray trail, $kT = 0.98_{-0.07}^{+0.06} \text{ keV}$ for model “Trail 2T”, is significantly hotter than the IGM gas to the south. Also, the abundance $A = 0.2 \pm 0.1 Z_{\odot}$ is low, marginally consistent with that found for the intragroup gas.

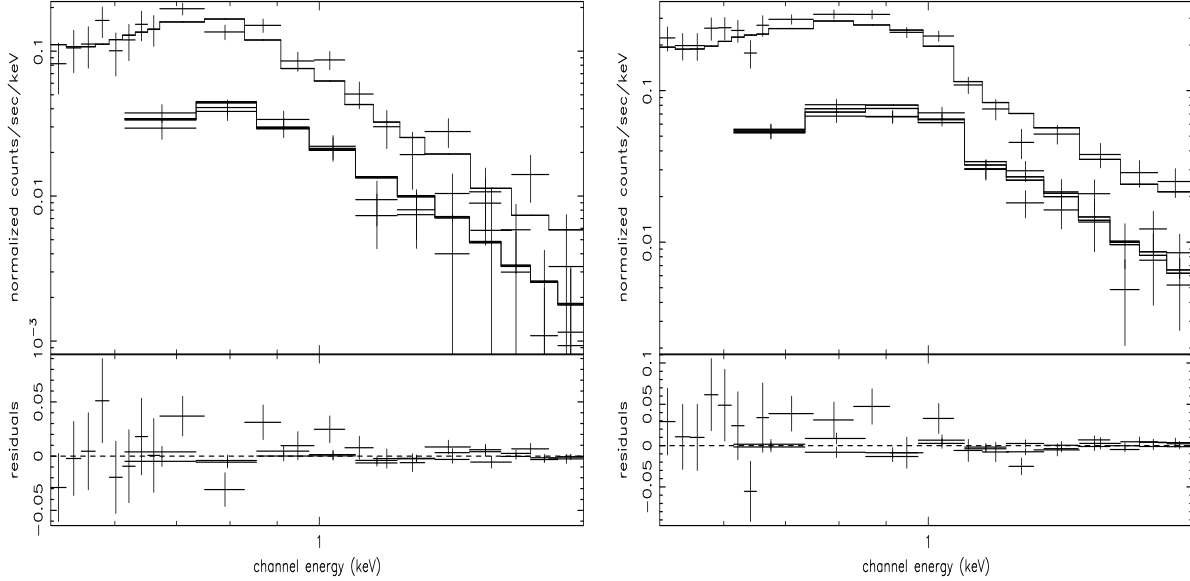


Fig. 4.— (left) Best simultaneous single temperature APEC model fit to MOS1, MOS2, and PN data for the undisturbed Pavo IGM, extracted from the southern rectangular region shown in Figure 2, with temperature $kT = 0.50^{+0.06}_{-0.05}$ keV, abundance $A = 0.05^{+0.03}_{-0.02} Z_{\odot}$, and fixed Galactic absorption $n_{\text{H}} = 4.97 \times 10^{20} \text{ cm}^{-2}$ (NED). (right) Best simultaneous two component APEC model fit to the X-ray trail extracted from the northwestern rectangular region between galaxies NGC 6876 and NGC 6872 in Figure 2. The X-ray trail component has temperature $0.98^{+0.06}_{-0.07}$ keV and abundance $0.2 \pm 0.1 Z_{\odot}$, while the background IGM component is fixed by the IGM model shown in the left panel and listed in Table 1.

3.2.2. Spectral Properties of NGC 6876 and NGC 6872

Our spectral fits for the galaxies NGC 6876 and NGC 6872 are summarized in Table 2. A single temperature APEC model with fixed Galactic absorption (model “NGC 6876, main 1Ta”) is a poor fit to our data for the central $\sim 1'$ of NGC 6876. The fit is improved if we allow the absorbing column to vary (model “NGC 6876, main 1Tb”) and is in excellent agreement with the single temperature model results of Buote & Fabian (1998) who find a temperature $kT \sim 0.88^{+0.15}_{-0.25}$ keV, abundance $A = 0.14^{+0.57}_{-0.07} Z_{\odot}$, and absorbing column $n_{\text{H}} = 2^{+4}_{-1} \times 10^{21} \text{ cm}^{-3}$; however, the χ^2/dof (179/91) for our fit is still large. Our data for both the main (62''.7) and extended (99''.8 with NGC 6877 removed) circular extraction regions are well represented by a two temperature APEC model where the abundances for each temperature component are constrained to vary together. The absorption is again fixed at

⁴see <http://heasarc.gsfc.nasa.gov/>, Archives & Software, nH:Column Density

the Galactic value. We find low (high) temperature components 0.76 ± 0.02 keV (2.3 ± 0.4 keV) with abundance $1.9_{-0.5}^{+1.2} Z_{\odot}$ for the central $1'$ main region and 0.75 ± 0.02 (1.6 ± 0.1) keV with abundance $0.95 \pm 0.3 Z_{\odot}$ for the extended ($\sim 1'.7$) extraction region, respectively. Such near solar or super solar abundances are expected in large elliptical galaxies (Brighenti & Mathews 1999; Buote 2002). Our results are again in good agreement with the two temperature Mekal model fits of ASCA data by Buote & Fabian (1998) who found temperatures $kT = 0.90 \pm 0.14$ and $kT > 1.5$ keV with abundance $0.27_{-0.17}^{+0.66}$ for a $2'$ region surrounding NGC 6876 (similar to our “extended” region, but including NGC 6877 given ASCA’s low spatial resolution). In the left panel of Figure 5 we show the spectrum and our two temperature best fit to the extended ($1'.7$) region of NGC 6876.

In the right panel of Figure 5, we show the spectrum and best fit model for the central $1'$ (bulge) region of the spiral galaxy, NGC 6872, at the northwestern end of the X-ray trail. Because of our limited statistics, we cannot constrain all the spectral parameters in our fits. We again fix the absorption at the Galactic value. A simple power law model is unable to fit the data, giving $\chi^2/\text{dof} = 123/44$ for photon index $\Gamma = 2.7$. A better, but still unacceptable,

Table 2. Spectral Fits to NGC 6876 and NGC 6872

Region	MOS1, MOS2, PN source counts	Γ	kT_1 keV	kT_2 keV	A Z_{\odot}	χ^2/dof
NGC 6872						
bulgeA	241, 282, 594	$2.0_{-0.4}^{+0.3}$	$0.65_{-0.06}^{+0.07}$...	1.0^{f}	48/42
bulgeB	241, 282, 594	$1.3_{-0.2}^{+0.3}$	0.65 ± 0.05	...	0.2^{f}	45/42
NGC 6876						
main 1Ta	1715, 1923, 3369	...	0.82 ± 0.01	...	0.25 ± 0.03	237/92
main 1Tb	1715, 1923, 3369	...	0.77 ± 0.2	...	0.25 ± 0.04	179/91
main 2T	1715, 1923, 3369	...	0.76 ± 0.02	2.3 ± 0.4	$1.9_{-0.5}^{+1.2}$	107/93
extended 2T	2219, 2495, 4377	...	0.75 ± 0.02	1.6 ± 0.1	0.95 ± 0.3	102.3/90

Note. — Extraction regions are circular with radii $58''.6$, $62''.7$, and $99''.7$ for the NGC 6872 “bulge”, NGC 6876 “main”, and NGC 6876 “extended” models, respectively. Superscript “f” denotes a fixed parameter. Absorption is fixed at the Galactic value ($n_{\text{H}} = 4.97 \times 10^{20} \text{ cm}^{-2}$) for all but model “main 1Tb” where it is fit ($n_{\text{H}} = 1.4_{-0.3}^{+0.2} \times 10^{21} \text{ cm}^{-2}$). All spectral fits use the $0.5 - 5$ keV bandpass.

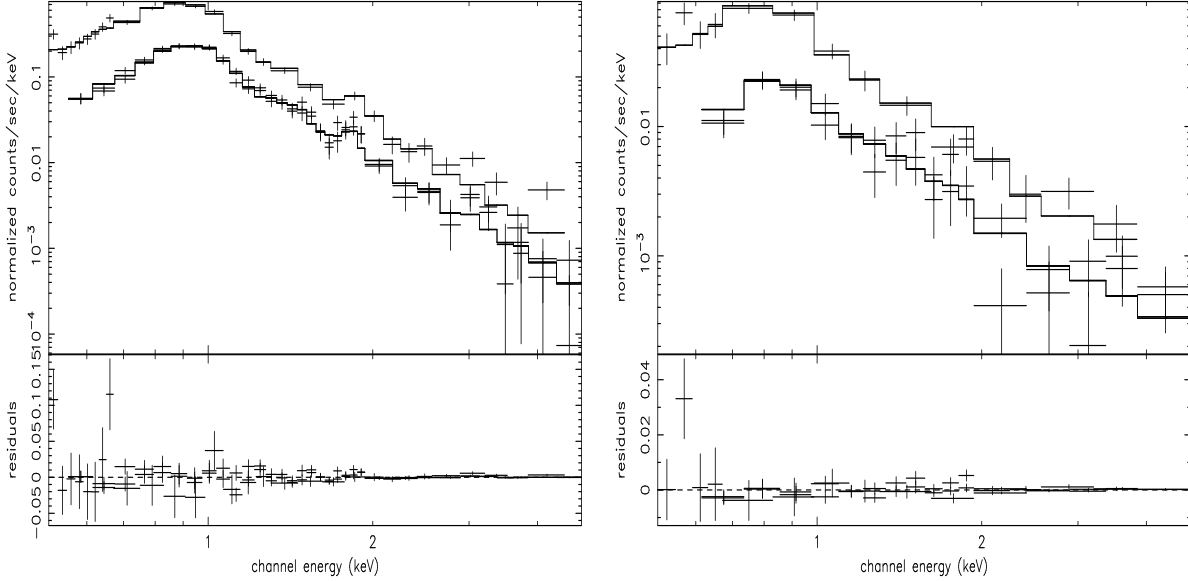


Fig. 5.— (left) Best simultaneous two temperature APEC model fit to MOS1, MOS2 and PN data for the extended emission from NGC 6876 in a circular aperture of radius $99''.7$ with a $10''$ circular region around NGC 6877 excluded. Absorption is fixed at the Galactic value and the abundance is assumed to be the same for both temperature components. (right) Best simultaneous two component APEC plus power law model fit to MOS1, MOS2 and PN data for a $58''.6$ circular aperture encircling the central region of the spiral NGC 6872 with fixed Galactic absorption and solar abundances.

fit is found using a thermal APEC model, yielding $kT = 0.75 \pm 0.05$ keV and abundance 0.06 ± 0.02 ($\chi^2/\text{dof} = 81/43$). We do find acceptable fits using a power law plus APEC model for both fixed solar abundance (model “bulgeA” with $\chi^2/\text{dof} = 48/42$) and fixed low abundance $A = 0.2 Z_\odot$ (model “bulgeB” with $\chi^2/\text{dof} = 45/42$), suggesting the presence of hot gas. We find the gas temperature ($kT = 0.65$) insensitive to the choice of abundance over this range; while the photon index for the power law component in the fits decreases with decreasing abundance from $\Gamma \sim 2$ (model “bulgeA”) to $\Gamma \sim 1.3$ (model “bulgeB”). This range of values is characteristic of those expected for unresolved X-ray point sources or a possible AGN (Ptak et al. 1999).

3.2.3. X-ray Luminosities

Once the surface brightness and spectral properties of the Pavo IGM, trail and galaxies have been determined, we can determine their luminosities. To compare our results for the Pavo group with those in recent surveys (Osmond & Ponman 2004, Mulchaey et al. 2003), we

determine the group luminosity by integrating the two component β -model fit to the surface brightness shown in Figure 3 that includes the central, dominant elliptical galaxy NGC 6876, but excludes all other sources. We find a $0.5 - 2$ keV luminosity within $r = 120$ kpc (the extent of the surface brightness fit) of $\log L_X = 41.8 \text{ erg s}^{-1}$. If we extrapolate our β -model fit to the characteristic radius r_{500} ,

$$r_{500} = \left(\frac{124}{H_0} \right) \left(\frac{T_X}{10 \text{ keV}} \right)^{1/2} \text{Mpc} \quad (1)$$

determined from simulations (Evrard et al. 1996) with T_X the temperature in keV and H_0 the Hubble parameter, we find $r_{500} = 0.37$ Mpc and $\log L_X(r_{500}) = 42.5 \text{ erg s}^{-1}$. This is similar to group luminosities found by Osmond & Ponman (2004) who find a mean $\log L_X(r_{500}) = 42.55 \text{ erg s}^{-1}$ for their group sample. However, since our β -model fit range was restricted to $r \lesssim 0.3r_{500}$ and the slopes of β -models in groups have been shown to steepen ($\beta \sim 0.4 - 0.5$) at larger radii (Osmond & Ponman 2004), our extrapolated luminosity $L_X(r_{500})$ may be biased somewhat high.

The observed fluxes and intrinsic luminosities for the northwestern (trail) region, as shown in Figure 2, and the two large galaxies, NGC 6876 and NGC 6872, are summarized in Table 3 for the best fit models. The total flux from the trail region is $3.2 \times 10^{-13} \text{ erg s}^{-1} \text{ cm}^{-2}$ ($0.5 - 2$ keV, soft) and $3.0 \times 10^{-14} \text{ erg s}^{-1} \text{ cm}^{-2}$ ($2 - 10$ keV, hard). Taking the distance to the dominant elliptical galaxy NGC 6876 ($D = 53.5$ Mpc) as representative of that to the Pavo group, this implies an intrinsic soft band (hard band) total luminosity of $\sim 1.3 \times 10^{41} \text{ erg s}^{-1}$ ($\sim 1.1 \times 10^{40} \text{ erg s}^{-1}$) for the region. The expected Pavo IGM background flux and luminosity, denoted as “IGM” in Table 3, are determined from the rectangular southern (IGM) region measurements. The IGM emission is dominated by soft emission, with the ratio of soft to hard band fluxes $\gtrsim 30$. After subtracting the IGM emission component, the remaining flux attributed to the X-ray trail, denoted “Trail” in Table 3, is $1.6 \times 10^{-13} \text{ erg s}^{-1} \text{ cm}^{-2}$ ($2.5 \times 10^{-14} \text{ erg s}^{-1} \text{ cm}^{-2}$) in the soft (hard) bandpass, respectively. The corresponding intrinsic soft (hard) band luminosity is $6.6 \times 10^{40} \text{ erg s}^{-1}$ ($9 \times 10^{39} \text{ erg s}^{-1}$). While the soft band luminosity from the trail component is comparable to that in the IGM component in this region, the hard band trail component is five times larger, consistent with the observed temperatures.

Our measured $0.5 - 2$ keV luminosity for the dominant elliptical galaxy NGC 6876 using the $99''.7$ aperture ($L_X = 2.4 \times 10^{41} \text{ erg s}^{-1}$) is in excellent agreement with the ROSAT PSPC results of O’Sullivan et al. (2001) who find $L_X = 2.6 \times 10^{41} \text{ erg s}^{-1}$ after correction to our assumed 53.5 Mpc distance. However, the absorbed flux we find for the spiral NGC 6872, $1.7 \times 10^{-13} \text{ erg s}^{-1} \text{ cm}^{-2}$ (corrected to the Einstein $0.2 - 4$ keV bandpass), is a factor ~ 5 smaller than the $8.66 \times 10^{-13} \text{ erg s}^{-1} \text{ cm}^{-2}$ found using Einstein data (Fabbiano et al. 1992; Shapley et al. 2001). This difference is due in part to our focus on the central $1'$ of the

Table 3. Observed X-ray Fluxes and Intrinsic Luminosities

Region/ component	Flux (0.5 – 2 kev) $10^{-13} \text{ erg s}^{-1} \text{ cm}^{-2}$	Flux (2 – 10 kev) $10^{-13} \text{ erg s}^{-1} \text{ cm}^{-2}$	$L_X(0.5 – 2 \text{ kev})$ $10^{40} \text{ erg s}^{-1}$	$L_X(2 – 10 \text{ kev})$ $10^{40} \text{ erg s}^{-1}$
Trail 2T	3.2	0.30	13.3	1.1
IGM	1.6	0.05	6.7	0.2
Trail	1.6	0.25	6.6	0.9
NGC 6872				
bulgeA	1.2	0.8	4.9	2.9
power law			2.4	2.8
thermal			2.5	0.07
bulgeB	1.1	1.1	4.6	4.0
power law			1.2	3.8
thermal			3.4	0.15
NGC 6876				
main 1Tb	4.5	0.4	24.4	1.6
main 2T	4.5	1.0	17.9	3.8
cool comp			13.6	0.6
hot comp			4.3	3.2
extended 2T	5.9	0.96	23.5	3.7
cool comp			15.3	0.7
hot comp			8.2	3.0

Note. — Fluxes are observed fluxes for the region/model listed in Tables 1 and 2. All luminosities are intrinsic, i.e. corrected for absorption, with the absorbing column taken to be Galactic ($n_{\text{H}} = 4.97 \times 10^{20} \text{ cm}^{-2}$) for all but the model “main 1Tb”, where the luminosity is corrected for absorption using $n_{\text{H}} = 1.4 \pm 0.2 \times 10^{21} \text{ cm}^{-2}$ taken from the fit. The trail region is rectangular with dimension $4'.35 \times 5'.9$; while the regions for the galaxies are circular with radii $58''.6$, $62''.7$, and $99''.7$ for the NGC 6872 bulge, NGC 6876 main, and NGC 6876 extended models, respectively. Identified point sources have been subtracted including a $10''$ circular region around NGC 6877.

galaxy, excluding contributions from IC 4970, resolved point sources and emission from the outer extensions of the tidally distorted spiral arms that would have been included in the Einstein measurement. As shown in Table 3, we find an intrinsic $2 - 10$ keV luminosity for the central region of the spiral galaxy NGC 6872 of 2.9×10^{40} erg s $^{-1}$ for $A = 1.0 Z_{\odot}$ (4.0×10^{40} erg s $^{-1}$ for $A = 0.2 Z_{\odot}$), dominated by the power law component of the model. Since the X-ray luminosity of low mass X-ray binaries (LMXB’s) scales with the total stellar mass of the galaxy, they contribute at most \sim a few $\times 10^{39}$ erg s $^{-1}$ to the integrated $2 - 10$ keV luminosity of the spiral NGC 6872 (Gilfanov 2004; Grimm et al. 2002). On the other hand, if the hard band luminosity is due to high mass X-ray binaries (HMXB’s), it provides a measure of the current star formation rate (sfr) in the galaxy (Gilfanov et al. 2003). Using the $L_X - sfr$ relation, with our measured $2 - 10$ keV luminosity, we predict a star formation rate of $4.3 M_{\odot}$ yr $^{-1}$ ($6.0 M_{\odot}$ yr $^{-1}$), respectively, for the above two models, consistent with the upper limit ($sfr \lesssim 5.6 M_{\odot}$ yr $^{-1}$) found by Mihos et al. (1993) using the $L_{\text{FIR}} - sfr$ relation. They argue, however, that the low H α luminosity found in NGC 6872 suggests that the star formation rate may be much lower. An alternative explanation may be that part of the hard band luminosity comes from a point source, possibly near the center of the spiral NGC 6872. Such ultra-luminous sources (ULX’s) appear to be quite common in galaxies. Colbert & Mushotzky (1999) found that 54% of a sample of 31 nearby face-on spirals and ellipticals contained such near-nuclear point sources, with $0.2 - 4$ keV luminosities up to $\sim 10^{40}$ keV. We do identify an X-ray point source in the $0.5 - 10$ keV band consistent with the optical center of NGC 6872; however because of the energy dependent broadening of the off-axis point spread function in the MOS detectors (the radius for 90% encircled energy at 5 keV for a source 8’ off axis is $\sim 50''$; XMM-Newton User’s Handbook⁵), we would expect the hard emission to be distributed over much of the extraction region, as is seen.

3.2.4. X-ray Properties of Other Pavo Galaxies

We briefly comment on the X-ray properties, listed in Table 4, of the other three galaxies detected in X-rays (NGC 6877, NGC 6880, and IC 4970) shown in Figure 1. The X-ray emission observed from these three galaxies is too faint to formally fit spectra. Instead we measure X-ray counts in $10''$ ($14''$) circular source regions for NGC 6880 and NGC 6877 (IC 4970) in the $0.5 - 2$ keV and $2 - 10$ keV energy bands. Local backgrounds are determined from an annular ring about each source. We then characterize the emission by computing hardness ratios defined by $(H - S)/(H + S)$, where S and H are the net source counts observed in the $0.5 - 2$ keV and $2 - 10$ keV energy bands, respectively, and corrected for

⁵http://xmm.vilspa.esa.es/external/xmm_user_support/documentation/uhb/index.html

telescope vignetting. We find that the spectra of NGC 6877 and NGC 6880 are soft, with the hard band counts consistent with background (within the large statistical errors), yielding hardness ratios ~ -0.9 , similar to that found in normal galaxies (including NGC 6876); while emission from IC 4970 is hard (hardness ratio of ~ 0.4), indicative of a nuclear starburst or active galactic nucleus (AGN). In Table 4 we give luminosities for each source derived using spectra consistent with the observed hardness ratios. The observed hardness ratios for NGC 6877 and NGC 6880 are consistent with a 1 keV Raymond-Smith plasma model with fixed solar abundance and Galactic absorption. Decreasing the temperature to 0.5 keV in these models decreases the estimated total 0.5 – 10 keV luminosities by $\lesssim 10\%$. The hardness ratio for IC 4970 is consistent with a power law model with photon index $\Gamma \sim 1.5$, typical of sources with nuclear activity (Ptak et al. 1999), and hydrogen absorbing column $n_H \sim 1.2 \times 10^{21} \text{ cm}^{-2}$. Nuclear activity is expected in galaxies undergoing an off-axis collision, such as the one indicated by the tidal stellar bridge between IC 4970 and the northern spiral arm of NGC 6872 (seen in Figure 1), as gas from the inner disk of the colliding galaxy is driven towards its center, either inducing a starburst or feeding a central black hole (Kannappan et al. 2004). If, however, the X-ray emission is due to HMXB’s produced in a recent starburst, the 2 – 10 keV luminosity implies a star formation rate of $\sim 9 M_\odot \text{ yr}^{-1}$ (Gilfanov et al. 2003).

Table 4. X-ray Properties for Other Pavo Galaxies

Galaxy	Net Counts 0.5 – 10 keV	Hardness Ratio	$L_X(0.5 – 2 \text{ kev})$	$L_X(2 – 10 \text{ kev})$
			$10^{40} \text{ erg s}^{-1}$	$10^{40} \text{ erg s}^{-1}$
NGC 6880	68 ± 20	-0.9 ± 0.1	0.14	0.02
NGC 6877	61 ± 25	-0.7 ± 0.3	0.13	0.015
IC 4970	554 ± 62	0.4 ± 0.1	2.3	6

Note. — Net counts are background-subtracted source counts corrected for telescope vignetting and summed over MOS1, MOS2 and PN detectors. Estimated luminosities assume a 1 keV Raymond-Smith plasma model with solar abundance and Galactic absorption for NGC 6880 and NGC 6877 and an absorbed power law model with photon index 1.5 and absorbing column $1.2 \times 10^{21} \text{ cm}^{-2}$ for IC 4970, chosen to match the observed hardness ratios. The distance to the Pavo group, $D = 53.5 \text{ Mpc}$, is taken as representative for the galaxies.

3.3. Electron Densities and Gas Mass Estimates

To characterize the X-ray emitting gas in the trail between NGC 6876 and NGC 6872, we use the spectral and surface brightness properties to estimate the electron density and X-ray gas masses in the enhanced emission trail, the undisturbed IGM, and the dominant elliptical NGC 6876. We assume that the gas in the X-ray trail uniformly fills a cylindrical region of radius 33.3 kpc (130''.6) and projected length $l_p = 90.2$ kpc (353''.6). The physical length of the trail and, thus, the volume occupied by the hot trail gas depend on the cosine of the angle ($u = \cos(\xi)$) that the motion of the spiral NGC 6872 makes with respect to the plane of the sky. We use the XSPEC spectral normalization of the 1 keV (trail) component to derive a mean electron density and estimated total gas mass in the trail of $n_{\text{trail}} \sim 1.1 \times 10^{-3} u^{1/2} \text{ cm}^{-3}$ and $M \sim 10^{10} u^{-1/2} M_{\odot}$. We determine the IGM density from our fits to the surface brightness profile, shown in Figure 2, using the second (IGM) component of the two component β -model, that dominates away from the trail at distances $\gtrsim 35$ kpc from the center of the elliptical. We find a central electron density of $1.3 \times 10^{-3} \text{ cm}^{-3}$ for the IGM component. We then take the IGM electron density computed from this β -model at the center of the trail cylinder ($r = 78u^{-1}$ kpc from NGC 6876) as representative of the mean electron density of the undisturbed IGM in that volume. In Figure 6 we plot the ratio α of the mean gas density in the trail (n_{trail}) to that in the IGM (n_{IGM}) as a function of u . For all but the largest angles ($\xi > 70^\circ$), $\alpha \lesssim 2$ such that the overdensity in the trail is $\lesssim 1$.

For the elliptical galaxy NGC 6876, we use the galaxy component of the β -model fit to the surface brightness profile in Figure 2, that dominates at small radii, to calculate the central electron density and integrated gas mass within 16 kpc (NGC 6876 main) and 25.4 kpc (NGC 6876 extended) spherical volumes. We find a central electron density of $\sim 2 \times 10^{-2} \text{ cm}^{-3}$ and hot gas masses of $\sim 1.7 \times 10^9 M_{\odot}$ ($\sim 3.4 \times 10^9 M_{\odot}$) within the central 16 kpc (extended 25.4 kpc) regions. However, the errors on these estimates are large, due to uncertainties in the central surface brightness caused by our limited statistics and to uncertainties in the gas metal abundance that influence the value we adopt for the 0.5–2 keV emissivity ($\Lambda \sim 1.9 \times 10^{-23} \text{ erg cm}^3 \text{ s}^{-1}$).

4. On the Nature and Origin of the Trail

The observation of a wake or trail behind a galaxy is one of the few ways known to determine the direction of a galaxy’s motion in the plane of the sky and thus constrain its dynamical motion through the group or cluster. In this case the direction and extent of the trail between NGC 6876 and NGC 6872, shown in Figures 1 and 2, indicate that the spiral NGC 6872 has recently accomplished a fly-by of the dominant elliptical NGC 6876.

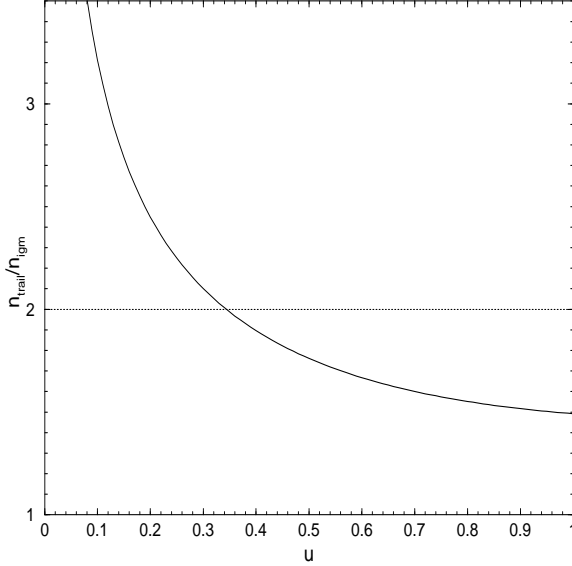


Fig. 6.— Dependence of the ratio α of mean densities for trail (n_{trail}) and IGM (n_{IGM}) gas on the cosine u of the angle of motion of NGC 6872 with respect to the plane of the sky. The horizontal line denotes $\alpha = 2$.

Since the speed of sound in the 0.5 keV Pavo group gas is $\sim 365 \text{ km s}^{-1}$ and assuming the central elliptical NGC 6876 is at rest relative to the IGM, the relative radial velocity ($v_r = 849 \pm 28 \text{ km s}^{-1}$, Martimbeau & Huchra 2004) between NGC 6872 and NGC 6876 suggests that the motion through the group gas is supersonic (Mach $M \gtrsim 2.3$). Key observations that need to be explained by any model are the length of the trail and the density, temperature and abundance of gas in the trail relative to that of the surrounding IGM.

Four possible physical mechanisms might contribute to the formation of the observed X-ray trail during such a fly-by event. The X-ray trail might be :

- gas tidally stripped from either NGC 6876 or NGC 6872, during the close encounter of the two systems.
- IGM material gravitationally focused into a Bondi-Hoyle wake (Bondi & Hoyle 1944; Bondi 1952; Hunt 1971; Ruderman & Speigel 1971) behind NGC 6872, as the IGM gas flows past the large spiral.
- galaxy ISM stripped from the spiral NGC 6872 by ram pressure (Gunn & Gott 1972), as the galaxy passed through the densest part of the Pavo IGM.
- gas stripped from NGC 6872 by turbulent viscosity (Nulsen 1982), due to the supersonic

motion of the spiral through the Pavo IGM, that is then thermally mixed with the ambient group gas.

Identification of the dominant process in the formation of the trail may not be easy, since all of these processes may act together to some degree during the passage of the spiral galaxy through the core of the group. We discuss each of these mechanisms below.

4.1. Tidal Interactions

Tidal interactions between the spiral NGC 6872 and the dominant group elliptical NGC 6876 during the fly-by, not just between the spiral and its small companion galaxy IC 4970 (Mihos et al. 1993; Horellou & Koribalski 2003), may well have contributed to the extended stellar tidal tails in NGC 6872. These stellar tidal tails stretch $\sim 2'$ (~ 30 kpc) to the east and west of its bulge (see Figure 1) and have associated with them $\sim 1.4 \times 10^{10} M_\odot$ (distance corrected to 53.5 Mpc) of HI gas (Horellou & Booth 1997; Horellou & Koribalski 2003). However, since tidal interactions affect gas and stars similarly and tend to be less effective for high speed encounters, they are unlikely to be the dominant process at work in the formation of the X-ray trail. If the $\sim 10^{10} M_\odot$ of hot gas in the X-ray trail originated in NGC 6872, it would represent more than 40% of the original gas mass in the galaxy. It is unlikely that tidal forces would displace that much hot gas without there also being evidence in the stellar or HI gas distributions of stars or cool gas displaced toward the region of the X-ray trail. Similarly, the gas cannot have come from the elliptical NGC 6876 in the interaction. The mass of gas in the X-ray trail is a factor $\gtrsim 3$ greater than the hot gas mass retained (within 25 kpc) by the dominant elliptical NGC 6876. If tidal interactions were that efficient in removing gas from the galaxy, one would expect similar distortions in the distribution of the stars, that are not seen. Also the heavy element abundance of gas in the trail is much lower than that measured in NGC 6876.

4.2. Bondi-Hoyle Wake

A second possibility is that the trail is a Bondi-Hoyle wake, where the group IGM is adiabatically compressed and heated, due to the gravitational focusing of the surrounding IGM by NGC 6872's gravitational potential, during the passage of the spiral through the group core. Qualitatively the fact that the measured heavy element abundance of gas in the trail is low, consistent with that of the Pavo IGM, rather than the near solar or super solar abundances expected for galactic gas or gas from a superwind, favors the interpretation of the

trail as a wake, consisting primarily of IGM material. The observed density in the trail (see Figure 6) is also reasonable, since adiabatic compression can readily produce overdensities of order unity.

Of more concern are the dimensions of the tail, i.e. whether gravitational focusing by the spiral can produce significant density perturbations that extend for $\gtrsim 90$ kpc behind the galaxy. The characteristic length scale for gas to be drawn into the wake is given by the Bondi-Hoyle accretion radius R_A , whose analytical form depends critically on whether the relative velocity of the galaxy v with respect to the surrounding medium is subsonic, where adiabatic gas infall dominates, or highly supersonic, where the accretion process is dominated by the dynamical motion of the gas (Bondi 1952). In the extreme subsonic regime ($v \ll s_{\text{IGM}}$, where s_{IGM} is the speed of sound in the surrounding medium), the accretion radius is given by $R_A = 2GM_g/s_{\text{IGM}}^2$, where G is the gravitational constant and M_g the accreting galaxy's (total) mass, while for hypersonic velocities ($v \gg s_{\text{IGM}}$) $R_A = 2GM_g/v^2$. Previous analyses at intermediate velocities appropriate for galaxies moving in groups or clusters have either used numerical simulations of highly idealized accretors, i.e. a gravitating point source (e.g. Bondi 1952, Hunt 1971) or totally absorbing sphere (e.g. Ruffert 1994), or have limited the accretors to slowly moving systems (Mach number $M \leq 1$), where the size of the galaxy is smaller than the accretion radius (Sakellou 2000). These results are not directly applicable to the trail we observe.

We can obtain an exact solution to the linearized flow equations for adiabatic motion, given in the Appendix, by convolving the Greens function for the equations, i.e. the solution for a gravitating point source moving supersonically through a uniform medium found by Ruderman & Spiegel (1971), with the density distribution for more realistic galaxy potentials. In the currently favored cosmologies, simulations show that the gravitational potential for galaxies is dominated by dark matter. Thus the scale for Bondi accretion is set by the mass distribution of the dark matter halo, whose density distribution, even for spirals, is well represented by the spherically symmetric NFW form

$$\rho(r) = \frac{\rho_0}{\frac{r}{a}(1 + \frac{r}{a})^2} \quad (2)$$

where ρ_0 is the central dark matter density and a is the inner NFW radius (Navarro, Frenk & White 1995, 1996, 1997). In the Appendix we solve the linearized flow equations for an NFW gravitational potential, i.e. a gas free galaxy, moving supersonically through a uniform medium with sound speed s . In Figure 7, we show these solutions for the density perturbation $\delta\rho/\rho_{0g}$ on the accretion axis for Mach numbers $1.05 \leq M \leq 4$. Negative (positive) values for z/a denote downstream (upstream) values of the distance from the perturber along the accretion axis. Several features of Figure 7 are noteworthy. First we see a strong asymmetry

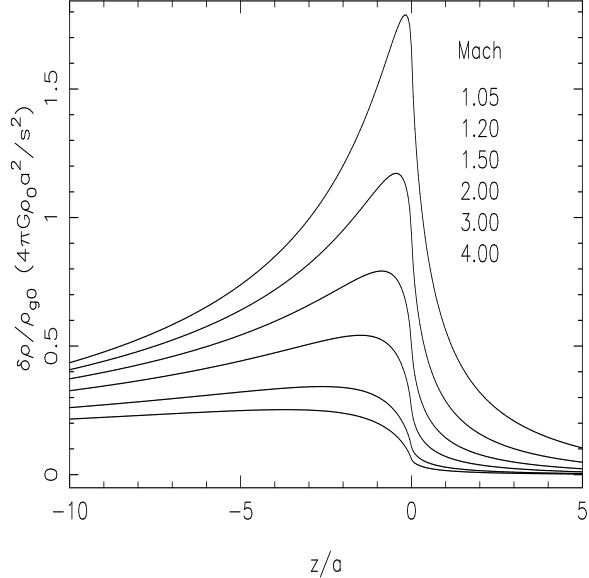


Fig. 7.— Density perturbation on the accretion axis produced by an NFW potential with central density ρ_0 and inner radius a , moving supersonically through a uniform medium with sound speed s . Negative values of z/a indicate distances along the accretion axis downstream of the perturber.

between the upstream and downstream values for the density perturbation, producing a wake of adiabatically compressed gas downstream of the galaxy. Secondly, as the speed of the halo through the medium increases, the peak of the density distribution moves somewhat downstream and its magnitude dramatically decreases, such that for the large Mach number ($M > 2.3$) expected for NGC 6872, the pile-up of accreted material near the center of the galaxy, predicted for subsonic motion (Sakellou 2000), does not occur. This is consistent with the low X-ray luminosities observed in the central region of the spiral. Third, as the Mach number increases the magnitude of the perturbation decreases with downstream distance much more slowly than for lower galaxy speeds relative to the medium. For example, for Mach $M \sim 3$ the density perturbation peaks at a downstream distance $z \sim 1.5a$ and decreases by $\lesssim 20\%$ at $z \sim 10a$. Thus for sufficiently large halos and high speeds, the density perturbation can be substantial at large downstream distances, producing a long wake comparable to what is seen.

Massive dark matter halos with large virial radii may be common for spirals. For example, dynamical models for the motion of gas in the Magellanic Streams associated with our Galaxy indicate a dark matter halo with radius > 100 kpc (Binney & Tremaine 1987). Such a large halo may be plausible for NGC 6872, especially if it is the center of a spiral-

dominated subgroup moving through Pavo. To estimate the size of the density perturbation expected for the motion of NGC 6872 through the Pavo IGM, we rewrite the scale factor for the perturbations in Figure 7 in terms of observable quantities, i.e.

$$\frac{4\pi G\rho_0 a^2}{s^2} = \frac{v_{\text{circ}}^2}{0.216 s_{\text{IGM}}^2} \quad (3)$$

where v_{circ} is the (maximum) rotation velocity for the spiral and $s = s_{\text{IGM}} \sim 365 \text{ km s}^{-1}$ is the sound speed in the undisturbed Pavo IGM. Although the rotation curve for NGC 6872 has not been measured, we can estimate the rotation velocity from the I-band or H-band Tully-Fisher relations (Pierce & Tully 1992). Using I-band (H-band) magnitudes 11.2 (8.64) from NED and distance $D = 53.5 \text{ Mpc}$ to NGC 6872, we find a rotation velocity $v_{\text{circ}} \sim 230(350) \text{ km s}^{-1}$ for the spiral. We caution the reader that the Tully-Fisher relation has not been calibrated in interacting systems like NGC 6872, so that optical measurements of the rotation curve in that system are needed to fully understand the kinematics and constrain the gravitational potential. However, the circular velocities we infer from the Tully-Fisher relation, $230 \lesssim v_{\text{circ}} \lesssim 350 \text{ km s}^{-1}$ are reasonable, comparable to those observed in more normal large spirals. Using the I-band result as a conservative estimate for the circular velocity, we determine the other NFW parameters for the spiral NGC 6872 by comparison with simulations (Bullock et al. 2001). We find a virial mass for NGC 6872 of $\sim 3 \times 10^{12} M_{\odot}$, the present epoch NFW concentration parameter $c \sim 15$, and the NFW inner radius $a \sim 20 \text{ kpc}$. Using these parameters for Mach $M = 3$ motion in Figure 7, the maximum IGM density perturbation (on the accretion axis) in the trail is estimated to be ~ 0.6 dropping to ~ 0.5 at $z \sim 10a \sim 200 \text{ kpc}$, comparable to the observed overdensity and length of the trail for angles $\xi \lesssim 45^\circ$ (see Figure 6).

A major concern is the effect such a large halo might have on the elliptical NGC 6876 during the close encounter of the two systems. Given the inferred large virial mass of the spiral NGC 6872, the halos of the two galaxies would most likely still be overlapping, yet the stellar and gas distributions of the elliptical do not appear strongly distorted. Similarly, it is unclear, without better numerical simulations, whether such a large halo for NGC 6872 would prevent the formation of its observed tidally-extended spiral arms either through interaction with the core group potential or with its companion, IC 4970. However, as indicated in Figure 7, the perturbation remains substantial downstream even for smaller a , that might result if the dark matter distribution for the galaxy has been modified by interaction with the group potential.

Another concern is the temperature rise observed in the trail. For the above overdensities of ~ 0.6 , conservation of entropy predicts a temperature ratio $T_{\text{trail}}/T_{\text{IGM}} \sim 1.4$, much less than that observed. To produce the observed ratio, $T_{\text{trail}}/T_{\text{IGM}} \sim 2$, would require a density

ratio $n_{\text{trail}}/n_{\text{IGM}} \sim 2.7$ and overdensity 1.7. Using our observed values for the density ratio in Figure 6 to fix the kinematical parameters for NGC 6872, we find an angle $\xi \sim 80^\circ$ and thus Mach number $M \sim 2.4$. From Figure 7 we see that an overdensity ~ 1.7 is possible provided the circular velocity of NGC 6872 is large ($\sim 350 \text{ km s}^{-1}$) and/or nonlinear effects become important, both assumptions testable in simulations, but then the inferred length of the observed trail ($\sim 500 \text{ kpc}$ for projected length $\sim 90 \text{ kpc}$) is probably too long. Thus it is unlikely that Bondi accretion alone can account for the properties of the observed trail. However, it may act in concert with other physical processes that can heat the gas in the trail.

Key observational signatures, detectable in deeper Chandra and XMM-Newton X-ray exposures, which are capable of distinguishing between gravitational focusing of the IGM into a Bondi-Hoyle wake and competing explanations for the trail, are the trail gas metal abundance and the temperature and density profiles along the trail. Since, in the Bondi-Hoyle wake scenario, the trail is composed only of gravitationally focused IGM gas, the trail gas abundance should match that in the undisturbed IGM. Entropy conservation also implies that the temperature and density profiles are correlated. The temperature of the trail is always hotter than the ambient IGM, due to adiabatic compression, with the peak temperature occurring near the spiral NGC 6872 where the density perturbation is greatest.

4.3. Ram-Pressure Stripping

A third possible explanation for the X-ray trail in this system is that it is a combination of Pavo IGM gas and ram-pressure-stripped ISM gas from NGC 6872 that has been shock heated and focused into the trail of enhanced X-ray emission (or wake) behind the spiral NGC 6872, due to the supersonic motion of the galaxy through the group IGM, during the spiral’s initial infall through the Pavo group center (near the dominant elliptical NGC 6876 and through the densest part of the Pavo IGM). To better understand whether this explanation is plausible, we compare our measured properties for gas in the X-ray trail to the results of simulations by Stevens et al. (1999) and those by Acreman et al. (2003) for galaxies moving supersonically through ICM gas. The simulations use a two dimensional PPM implementation of hydrodynamics with gravity and a simple model for mass replenishment from supernovae, to study the dependence of observables on cluster gas temperature, Mach number, and galaxy mass replenishment rate for a canonical elliptical galaxy of total mass $1.2 \times 10^{12} M_\odot$ moving at constant velocity through the cluster gas (Stevens et al. 1999), and on the galaxy gas halo size, galaxy mass, galaxy mass replenishment rate and infall radius for radial infall of a spherical galaxy through 2.7 keV cluster gas (Acreman et al. 2003). Our

data are most similar to the cool (1 keV) cluster simulations of Stevens et al. (1999). While the effects of the very different geometrical cross-section presented by the gas distributions in the spiral NGC 6872 are difficult to predict and require further simulation, one might expect that the gross properties of the wakes would be similar.

The three potentially visible features of a galaxy undergoing ram-pressure stripping, due to supersonic motion through the surrounding cluster gas, are a bow-shock preceding the galaxy, a cold front at the galaxy's leading edge, and an extended tail or wake trailing the galaxy. Of these, the bow-shock is the least visible and, in our case where the spiral NGC 6872 is observed far off axis in the detector, would not be expected to be seen. The trailing wake is the next most visible feature found in the simulations (Stevens et al. 1999; Acreman et al. 2003). Stevens et al. (1999) find that the most visible, densest wakes form behind galaxies in cool clusters, with high mass replenishment rates; while Acreman et al. (2003) find the wakes are most visible for galaxies with substantial initial gas content on their first passage through the cluster. Both conditions may hold in our case, since the Pavo group is cool, the trail morphology suggests a fly-by through the group center, and NGC 6872 has substantial HI gas along its tidally extended spiral arms.

Simulations by Stevens et al. (1999) suggest that ram-pressure stripping of the ISM in galaxies in cool clusters or groups may not be efficient, with mass retention factors between 30% for low mass replenishment rates, appropriate for galaxies with only an old population of stars, to 75% – 89% for higher mass replenishment rates more appropriate for galaxies with recent star formation. Recent star formation is observed in and at the ends of the tidally distorted spiral arms of NGC 6872 (Mihos et al. 1993), such that the latter case with less efficient stripping may be more applicable. Given that the mass of hot gas in the X-ray trail is $\sim 40\%$ of the HI mass measured in NGC 6872, this implies a mass retention factor of $\sim 60\%$, in agreement with the simulations. Stevens et al. (1999) also argue that the temperature of the wake can be hotter or cooler than the ambient cluster gas, depending on whether the wake consists primarily of shocked IGM gas or cooler ram-pressure stripped ISM gas. Our hotter temperature for the trail would imply that shock-heated IGM gas dominates, consistent with the observed low abundance ($\sim 0.2 Z_{\odot}$) of the trail gas. However, the small range of temperatures reported for their simulated wakes were all comparable to (within $\sim 10\%$) or less than the temperature of the surrounding ICM, rather than the factor ~ 2 higher temperature we observe.

The simulations of Acreman et al. (2003) provide insight into the expected luminosity and extent for trails produced by ram-pressure stripping. They find that the broadest and brightest wakes occur for galaxies undergoing their first core crossing of the cluster with simulated 0.3–8 keV luminosities for the wake at core crossing of $\log L_X \sim 40.6 - 41.3 \text{ erg s}^{-1}$.

This is comparable to the $\log L_X = 40.9 \text{ erg s}^{-1}$ we measure for the X-ray trail. They further find that a factor two or more enhancement in the surface brightness in the wake persists out to distances $\gtrsim 60 \text{ kpc}$ from the galaxy for times $\sim 700 \text{ Myr}$ after core crossing (see Figure 14, Acreman et al. 2003) for galaxies with extended gas halos, making the 90 kpc long trail we observe more plausible.

In addition to the large temperature difference between the IGM and gas in the trail, another discrepancy between the simulations and our observations is that all of the two dimensional simulations that input spherical β -model mass distributions for the gas in the simulated galaxies predict bright X-ray enhancements at the center of the galaxy due to gas in the wake falling back and accumulating in the central region. While X-ray emission is observed from the central region of NGC 6872, it is weak, far less than the orders of magnitude enhancement predicted by the simulations. This may be due to the different geometry and initial gas distribution of the two systems, may be an artifact of the two dimensional nature of the simulations (e.g., see Ruffert 1994), or may indicate the presence of additional physics (e.g. multiphase ISM, magnetic fields, nuclear feedback processes) that have not been included in the simulations. The discrepancies between our observations and the simulations may also be due in part to the limited spatial resolution of the simulations that makes it difficult to model well the effects of Kelvin-Helmholtz instabilities and turbulence on the stripping process.

4.4. Turbulent Viscous Stripping

The fourth explanation for the X-ray trail is that it was formed by turbulent viscous stripping of cold gas from the spiral NGC 6872, that is thermalized and then thermally mixed with the ambient Pavo IGM, during the galaxy’s supersonic motion past the group center. Since the mass loss rate due to turbulent viscous stripping is largely insensitive to the orientation of the galaxy as it moves through the IGM, this process may dominate over classic ram-pressure stripping in large spirals (Nulsen 1982). Numerical simulations of this system are needed to test this hypothesis in detail. However, we can employ simple conservation arguments to determine if the scenario is qualitatively feasible. We consider mass conservation, the turbulent-viscous stripping rate, energy conservation applied to the process of thermalization, and the constraint on the dimensions of the observed trail imposed by adiabatic expansion of the gas. All of these constraints depend on the angle ξ that the motion of NGC 6872 makes with respect to the plane of the sky, either directly through the velocity of the spiral or indirectly through the electron densities for gas in the IGM and the trail inferred from observations in Section 3.3. In Figure 8 we plot these constraints as a

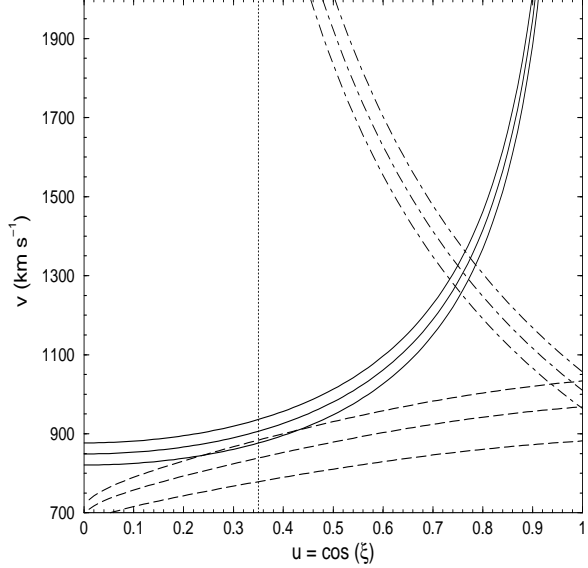


Fig. 8.— Constraints on the velocity of NGC 6872 in the turbulent viscous stripping model for the trail: measured radial velocity (solid line), energy conservation (long-dashed line, lower bound), trail dimensions and adiabatic expansion (dot-dashed line), mass conservation and turbulent viscous stripping rate (vertical dotted line, allowed values are to the right). Uncertainties in the constraints are denoted by thin lines of the same kind as the constraint, and are due to the uncertainties in the measured temperatures (long-dashed and dot-dashed lines) and measured radial velocity (solid line).

function of $u = \cos(\xi)$.

From mass conservation, the density of gas in the trail that was stripped from the spiral, n_{strip} , is given by $n_{\text{strip}} = (\alpha - 1)n_{\text{IGM}}$, where n_{IGM} is the density of the undisturbed IGM and $\alpha = n_{\text{trail}}/n_{\text{IGM}}$ is the ratio of trail to IGM gas densities. The rate at which mass would be stripped from a galaxy by turbulent viscosity, \dot{M}_{turb} , is given by

$$\dot{M}_{\text{turb}} \sim \pi R^2 \rho_{\text{IGM}} v f \quad (4)$$

where R is the radius of the gas disk (\sim radius of the trail), ρ_{IGM} is the density of the ambient IGM, v is the relative velocity of NGC 6872 with respect to the IGM, and f accounts for the reduction in the stripping rate when the galaxy's gravity becomes important (Nulsen 1982). The factor f can be written in terms of the circular velocity of the galaxy at the radius of the gas disk, $f = \min[v^2/v_{\text{cir}}^2(R), 1]$. Since the velocity of NGC 6872 through the IGM ($v \gtrsim v_r = 849 \text{ km s}^{-1}$) is larger than the estimated rotation velocity ($v_{\text{cir}} \sim 200 - 350 \text{ km s}^{-1}$) for the spiral, gravity does not significantly affect the stripping rate and $f \sim 1$. Integrating

over time in Equation 4, we see that turbulent viscous stripping can remove a gas mass from the galaxy approximately equal to the mass of undisturbed IGM gas originally contained in the trail volume. Turbulent-viscous stripping is efficient enough to produce the observed ratio of trail to IGM gas mass provided $\alpha \lesssim 2$. Given the measured densities found in Section 3.3, this restricts the angle of motion with respect to the plane of the sky, ξ , to angles less than 70° ($u > 0.34$, to the right of the dotted line in Figure 8).

Energy conservation also constrains the speed of the spiral galaxy through the IGM in this scenario. The trail is heated to 1 keV when the kinetic energy carried in the cold galaxy gas is thermalized by turbulent viscous stripping and the stripped gas mixed with the IGM. Ignoring any initial adiabatic expansion of the gas, energy conservation implies

$$\frac{\rho_{\text{strip}} v^2}{2} + \frac{3n_{\text{IGM}} k T_1}{2} \approx \frac{3n_{\text{trail}} k T_2}{2} \quad (5)$$

with ρ_{strip} the mass density of the stripped gas, v the relative velocity of the galaxy with respect to the IGM, and T_1 and T_2 the temperatures of the Pavo IGM before mixing and the X-ray trail after thermal mixing, respectively. Equation 5 can be conveniently rewritten in terms of the sound speeds s_{trail} and s_{IGM} for gas in the trail and IGM, respectively, and the ratio α of trail to IGM gas densities, yielding

$$v^2 \approx \frac{9}{5(\alpha - 1)} (\alpha s_{\text{trail}}^2 - s_{\text{IGM}}^2) \quad (6)$$

for gas with adiabatic index $\gamma = 5/3$. Since any initial work done by the gas, other dissipative forces and adiabatic expansion were neglected, Equation 5 (or 6) imposes a lower bound on NGC 6872’s velocity (shown as the long-dashed lines in Figure 8, where the uncertainties reflect the 90% CL uncertainties in the measured temperatures). The actual uncertainties inherent in our simple approximations are likely much larger.

Once the trail is formed, it is overpressured relative to the surrounding IGM and thus adiabatically expands and cools until the trail gas regains pressure equilibrium with its surroundings. During turbulent viscous stripping the entropy of the gas may change, either increasing, due to shocks caused by the supersonic motion of the galaxy through the IGM, or decreasing, as a result of the thermal mixing of stripped gas with the ambient group medium. Numerical simulations are needed to determine which effect dominates. However, observationally the trail appears to fade into the surrounding IGM background, so that the final entropy of the trail is most likely close to the initial entropy of the IGM gas. The trail ceases to be visible because, at pressure equilibrium, it has expanded back nearly to the temperature and density of its surroundings. The amount of broadening in the trail is thus determined by the pressure ratio between the trail gas and the surrounding IGM

$$\frac{r_{\text{max}}}{r_{\text{i}}} \approx \left(\frac{p_{\text{trail}}}{p_{\text{IGM}}} \right)^{1/2\gamma} = \left(\frac{T_{\text{trail}}}{\alpha T_{\text{IGM}}} \right)^{1/2\gamma} \quad (7)$$

where $r_{\max}(r_i)$ are the initial and maximum radial widths of the trail, γ is the adiabatic index, T_{trail} and T_{IGM} are the trail and IGM gas temperatures, respectively, and α is the ratio of trail to IGM gas densities. If we further assume that the adiabatic expansion of the trail proceeds at roughly the sound speed in the trail (s_{trail}), we can obtain an independent estimate of the galaxy velocity from the ratio of the physical length $l_t = l_p/u$, given in terms of the observed projected length l_p and cosine of the angle of motion $u = \cos(\xi)$ of NGC 6872 with respect to the plane of the sky, to its initial radial width r_i

$$v \sim \frac{l_t s_{\text{trail}}}{r_{\max}} \sim \frac{l_p s_{\text{trail}}}{u r_i} \left(\frac{T_{\text{trail}}}{\alpha T_{\text{IGM}}} \right)^{\frac{1}{2\gamma}}. \quad (8)$$

Equation 8 is shown in Figure 8 (dot-dashed line) for the measured projected trail length of 90 kpc, trail radial width of 33 kpc, and sound velocities in the trail and IGM of 511_{-19}^{+14} km s $^{-1}$ and 365_{-19}^{+21} km s $^{-1}$, respectively, corresponding to $0.98_{-0.07}^{+0.06}$ keV trail and $0.50_{-0.05}^{+0.06}$ keV IGM gas.

Finally, the galaxy velocity must satisfy the radial velocity constraint, $v = v_r / \sin(\xi)$, given by the solid line in Figure 8 for $v_r = 849 \pm 28$ km s $^{-1}$ (Martimbeau & Huchra 2004). Although these results need to be refined by hydrodynamical simulations, taken together these conditions allow us to estimate the velocity of NGC 6872 required to form the observed trail by turbulent-viscous stripping of the spiral. From Figure 8 we find these constraints are satisfied if NGC 6872 moves with a speed $v \sim 1300$ km s $^{-1}$ at an angle $\xi \sim 40^\circ$ with respect to the plane of the sky. Once the three dimensional motion of NGC 6872 is determined, we can complete the physical characterization of the trail. The ratio of trail to IGM gas densities is then $\alpha \sim 1.57$, such that 36% of the trail gas has been stripped from the spiral with the remaining 64% of the trail gas from the Pavo IGM. The mean density and total gas mass in the trail are then 9.5×10^{-4} cm $^{-3}$ and $1.1 \times 10^{10} M_\odot$. Given the observed projected length (~ 90 kpc) and inferred transverse velocity (1000 km s $^{-1}$) of NGC 6872 in the plane of the sky, the age of the trail would be ~ 90 Myr. We note that cooling by thermal conduction is unimportant for the trail. The timescale for thermal conduction (Sarazin 1988) across the 33 kpc radius of the trail at the unsuppressed Spitzer rate is ~ 230 Myr, much greater than the age of the trail, and if tangled magnetic fields similar to those found in clusters are also present in galaxy groups, the thermal conduction timescale may be 3 – 100 times longer (Markevitch et al. 2003).

There are several key signatures of turbulent viscous stripping that can be tested in future observations. (1) The predicted motion of NGC 6872 is highly supersonic relative to the Pavo group gas. This would produce a strong shock in front of the spiral galaxy that should be visible in future X-ray observations with XMM-Newton or Chandra, in a more favorable pointing with NGC 6872 closer to the telescope aimpoint. (2) The metal abundance measured in the trail should be intermediate between that in the NGC 6872 and the Pavo IGM, reflecting the mixture of gases in the trail. (3) Since the trail is overpressured

and adiabatically expands, a simple prediction of this scenario is that, as the distance from the spiral increases, the trail should broaden and become cooler, less dense and dimmer. In Figure 3 we see evidence that this may be the case. The difference between the surface brightness observed in the trail (northwest) region and IGM (southern) region decreases with increasing distance from the spiral, i.e. as one moves closer to the dominant elliptical NGC 6876. (4) The temperature profile along the trail as a function of distance from NGC 6872 is distinctive. Since the X-ray trail is heated as the kinetic energy carried in the stripped, cold galaxy gas is thermalized and mixed with the IGM, this model predicts a cooler temperature near NGC 6872 where the thermalization is incomplete, in contrast to the hotter temperatures expected for a Bondi-Hoyle wake. The temperature is predicted to rise initially with distance as thermalization and mixing is complete, and then decrease with the adiabatic expansion of the gas. (5) The observation of filamentary features in the trail, as suggested in Figure 1, would also favor turbulent-viscous stripping, since the parent cold gas clouds need not be uniformly distributed in the spiral. Furthermore, the interaction of the companion galaxy IC 4970 with NGC 6872 may also displace gas within the spiral, making it easier to be stripped.

While physically possible, the velocity 1300 km s^{-1} (Mach ~ 3.6) of NGC 6872 required to satisfy both the radial velocity constraint and the geometrical constraint in Equation 8, imposed by the dimensions of the trail, is unusually high for motion through a cool group. This is a result of the competing factors imposed by the long observed projected length of the trail and the rapid adiabatic expansion of the overpressured trail gas, at the speed of sound s_{trail} , after thermal mixing. However, as discussed in Section 4.2, the more likely physical situation is that Bondi-Hoyle gravitational focusing is also significant and acts to inhibit the adiabatic expansion of the trail gas. Thus the effective expansion velocity of the trail in Equation 8 decreases so that the time over which the trail is visible (trail age) increases, shifting the dot-dashed curve in Figure 8 to lower galaxy velocities.

5. Conclusions

The observation of X-ray wakes and trails behind galaxies in groups and clusters opens exciting new opportunities to constrain the dynamical motion of galaxies in these systems and to probe the physical processes that govern their interaction with the surrounding environment. In this paper we have presented the results of a 32.2 ks XMM-Newton observation of an X-ray trail spanning the full $8'.7 \times 4'$ projected area between the large spiral galaxy NGC 6872 and the dominant elliptical galaxy NGC 6876 in the Pavo group, the first observation of an X-ray trail produced by a spiral galaxy in a poor galaxy group.

In summary we found:

1. The $0.5 - 2$ keV surface brightness profile for the dominant elliptical NGC 6876 is well described by a β -model with core radius $r_c = 5$ kpc and index $\beta = 0.65$ within 10 kpc. Beyond 10 kpc the surface brightness becomes highly asymmetric with the profile to the south (away from the spiral NGC 6872) well described by the addition of a second Pavlo IGM component with $r_c = 50$ kpc, $\beta = 0.3$; while to the northwest (in the direction of NGC 6872) the surface brightness beyond ~ 20 kpc is constant or slowly rising, and by $r \sim 60$ kpc is a factor $\gtrsim 2$ higher than in the Pavlo IGM to the south.
2. Using a single temperature APEC model with Galactic absorption, we find a temperature and abundance for the undisturbed Pavlo IGM of $0.50_{-0.05}^{+0.06}$ keV and $0.05_{-0.02}^{+0.03} Z_\odot$, and a group $0.5 - 2$ keV luminosity (including NGC 6876) within a radius of 120 kpc of 6.3×10^{41} erg s $^{-1}$.
3. The spectrum of gas in the (northwest) X-ray trail region is well fit by a two temperature model with one component fixed by the Pavlo IGM background and the other varied to determine the properties of the X-ray gas in the trail. We find a temperature $0.98_{-0.07}^{+0.08}$ keV and abundance $0.2 \pm 0.1 Z_\odot$ for gas in the trail. The $0.5 - 2$ keV ($2 - 10$ keV) luminosity of the X-ray trail component from the $4'.35 \times 5'.9$ rectangular extraction region is 6.6×10^{40} erg s $^{-1}$ (9×10^{39} erg s $^{-1}$).
4. For the dominant elliptical galaxy, NGC 6876, the spectrum for a $99''.7$ circular region (excluding NGC 6877) is best fit by a two temperature APEC model with abundance $0.95 \pm 0.3 Z_\odot$ and temperatures 0.75 ± 0.02 and 1.6 ± 0.1 keV for fixed Galactic absorption. We find $0.5 - 2$ ($2 - 10$) luminosities of 2.4×10^{41} erg s $^{-1}$ (3.7×10^{40} erg s $^{-1}$), a central electron density of ~ 0.02 cm $^{-3}$, and hot gas mass $\sim 3.4 \times 10^9 M_\odot$.
5. The spectrum for the $58''.6$ central region of the spiral NGC 6872 is best fit using an APEC plus power law model with temperature $kT = 0.65 \pm 0.06$ keV and photon index $\Gamma = 2.0_{-0.4}^{+0.3}$ ($\Gamma = 1.3_{-0.2}^{+0.3}$) assuming fixed extremes for the abundance, $A = 1 Z_\odot$ ($A = 0.2 Z_\odot$), respectively. The $0.5 - 2$ keV luminosity from this region is 4.9×10^{40} erg s $^{-1}$ (4.6×10^{40} erg s $^{-1}$) for these models. The $2 - 10$ keV luminosity, 2.9×10^{40} erg s $^{-1}$ (4.0×10^{40} erg s $^{-1}$) is too high to be produced by LMXBs alone. If attributed to HMXBs, the $2 - 10$ keV luminosity predicts a star formation rate in the central $58''.6$ of the spiral NGC 6872 of $\sim 4.3 M_\odot$ yr $^{-1}$ ($\sim 6 M_\odot$ yr $^{-1}$).
6. The measured subsolar abundance for gas in the X-ray trail is similar to that of the undisturbed Pavlo IGM. However, better spectra are needed to measure abundances in

the spiral NGC 6872, as well as in the IGM and trail, to determine the origin of gas in the trail.

7. The trajectory for NGC 6872, inferred by the presence of the trail, suggests that tidal interactions with NGC 6876, as well as those from its interacting companion IC 4970, may have contributed to the tidal distortion of the galaxy’s spiral arms and HI gas distribution. These interactions also should be included in dynamical models of the spiral galaxy’s evolution.
8. A possible explanation for the X-ray trail is that it is thermally mixed Pavo IGM gas (64%) and ISM gas (36%) that has been stripped from NGC 6872 by turbulent viscosity as the spiral moves supersonically ($v \sim 1300 \text{ km s}^{-1}$) through the Pavo IGM at an angle $\xi \sim 40^\circ$ with respect to the plane of the sky, passing the Pavo group center (the elliptical NGC 6876) $\sim 130 \text{ Myr}$ ago. The dimming of the trail as the gas adiabatically expands can explain the $\sim 100 \text{ kpc}$ projected length of the trail. Better simulations that include the effects of turbulence on stripping processes are needed to model the complex dynamics of this system.
9. The mean electron density and total mass in the trail inferred from the data are dependent on the projection geometry. Assuming uniform filling of the cylindrical geometry and an angle $\xi \sim 40^\circ$, from the turbulent-viscous stripping model, for the motion of the spiral with respect to the plane of the sky, we find a mean electron density for gas in the X-ray trail of $9.5 \times 10^{-4} \text{ cm}^{-3}$ and total hot gas mass in the trail of $1.1 \times 10^{10} M_\odot$. Nonuniform filling, as suggested by the X-ray images, would increase (reduce) the density (mass) by factors $\eta^{-1/2}$ ($\eta^{1/2}$), respectively, where $\eta \leq 1$ is the filling factor.
10. Gravitational focusing of IGM gas into a Bondi-Hoyle wake due to the highly supersonic motion of NGC 6872 through the Pavo IGM may also be significant. Better X-ray observations are needed to measure the metal abundance and temperature profile near the trail head to distinguish between gravitational focusing and turbulent-viscous stripping as the dominant trail formation mechanism and to find the bow shock predicted by both models. Optical measurements are needed to measure the rotation curve in the spiral NGC 6872. Better numerical simulations are needed to constrain the properties of NGC 6872’s dark matter halo and thus set the scale for gravitational focusing in this system.

This work has been supported in part by NASA contract G03-4176A, and the Smithsonian Institution. MEM and LS also acknowledge support from the Radcliffe Institute for

Advanced Study at Harvard University. This work has made use of the NASA/IPAC Extragalactic Database (NED) which is operated by the Jet Propulsion Laboratory, California Institute of Technology, under contract with the National Aeronautics and Space Administration. We wish to thank John Huchra and Michael McCullough for useful discussions, and Ralph Kraft for help with the data.

A. Gas flow through an NFW potential

The model is of an “empty” (gas free) galaxy moving through an otherwise uniform gas. Cooling can be ignored, since the time for gas to pass through the wake is significantly shorter than its cooling time. The effect of gravity is treated as a perturbation, using linearized flow equations. This gives an accurate result when the fractional density perturbation is small, which is a marginal approximation in practice.

The full flow equations are

$$\frac{d\rho}{dt} + \rho \nabla \cdot \mathbf{v} = 0, \quad (\text{A1})$$

$$\rho \frac{d\mathbf{v}}{dt} = -\nabla p + \rho \mathbf{g} \quad (\text{A2})$$

and

$$S = \text{constant}, \quad (\text{A3})$$

where ρ , p , S and \mathbf{v} are the density, pressure, specific entropy and velocity, respectively, of the gas. The acceleration due to gravity is \mathbf{g} and the lagrangian derivative is $d/dt = \partial/\partial t + \mathbf{v} \cdot \nabla$. In a frame moving with the galaxy, the flow is steady ($\partial/\partial t = 0$). Gas properties at large distances from the galaxy are uniform and we denote them by subscript ‘0’. Treating the effect of gravity as a perturbation, we write $\rho = \rho_{g0} + \delta\rho$, $p = p_0 + \delta p$ and $\mathbf{v} = \mathbf{v}_0 + \delta\mathbf{v}$, and linearize the flow equations. Equation (A1) then gives

$$\mathbf{v}_0 \cdot \nabla f + \nabla \cdot \delta\mathbf{v} = 0, \quad (\text{A4})$$

where $f = \delta\rho/\rho_{g0}$ is the fractional density perturbation. Equation (A3) implies that $\delta p = s_0^2 \delta\rho$, where s_0 is the speed of sound in the unperturbed gas, so that the linearized form of equation (A2) can be written as

$$\mathbf{v}_0 \cdot \nabla \delta\mathbf{v} = -s_0^2 \nabla f + \mathbf{g}. \quad (\text{A5})$$

Eliminating $\delta\mathbf{v}$ between (A4) and (A5) gives

$$(\mathbf{v}_0 \cdot \nabla)^2 f - s_0^2 \nabla^2 f = -\nabla \cdot \mathbf{g} = 4\pi G \rho_*, \quad (\text{A6})$$

where ρ_* is the density of gravitating matter in the galaxy (the gas is assumed to have negligible gravity).

Equation (A6) for the density perturbation is linear, with the gravitating mass density as its source term. Its solution is conveniently expressed in terms of a Greens function, $q(\mathbf{r})$, a solution of

$$(\mathbf{v}_0 \cdot \nabla)^2 q - s_0^2 \nabla^2 q = 4\pi G M \delta(\mathbf{r}), \quad (\text{A7})$$

where $\delta(\mathbf{r})$ is the Dirac delta function. The solution of (A6) is then

$$f(\mathbf{r}) = \frac{1}{M} \int q(\mathbf{r} - \mathbf{r}') \rho_*(\mathbf{r}') d^3 \mathbf{r}'. \quad (\text{A8})$$

Equation (A7) is the linearized equation for the density perturbation due to a point mass, M , moving through a uniform, adiabatic gas (Ruderman & Spiegel 1971). For a point mass moving supersonically in the $+z$ direction, with Mach number $m = v_0/s_0$, its solution expressed in terms of the radius, r , and polar angle, θ , is

$$q(\mathbf{r}) = \frac{2GM}{s_0^2 r \sqrt{1 - m^2 \sin^2 \theta}}, \quad \text{for } \cos \theta < -\sqrt{1 - 1/m^2}$$

and $q(\mathbf{r}) = 0$ otherwise (outside the Mach cone). The solution for subsonic motion is formally half of this, but non-zero everywhere, so that the density perturbation is the same in front of and behind the perturber. We only consider the supersonic case below.

Using these results, the fractional density perturbation at a point on the z axis, at $\mathbf{r} = (0, 0, z)$, due to a galaxy moving at Mach m in the $+z$ direction is given by

$$f(z) = \int \frac{2G\rho_*(\mathbf{r}') d^3 \mathbf{r}'}{s_0^2 \sqrt{(z - z')^2 - (m^2 - 1)(x'^2 + y'^2)}},$$

integrated over the interior of the inverted Mach cone of $(0, 0, z)$ (i.e. the region defined by $z' - \sqrt{(m^2 - 1)(x'^2 + y'^2)} > z$). If the distribution of gravitating matter is spherically symmetric, with $\rho_*(\mathbf{r}') = \rho_*(r')$, then this can be integrated over the angular coordinates, giving

$$f(z) = \frac{4\pi G}{s_0^2} \int_0^\infty g(m, z/r') \rho_*(r') r' dr', \quad (\text{A9})$$

where

$$g(m, t) = \begin{cases} \frac{1}{m} \ln \left| \frac{m-t}{m+t} \right|, & t < -1, \\ \frac{1}{2m} \ln \frac{(m+1)(m-t)}{(m-1)(m+t)}, & -1 < t < 1, \\ 0, & t > 1. \end{cases}$$

Taking $\rho_*(r) = \rho_0/[(r/a)(1+r/a)^2]$ for $r/a < c$, appropriate to an NFW potential with inner radius a and concentration parameter c , equation (A9) gives

$$f(z) = \frac{4\pi G \rho_0 a^2}{s_0^2} \begin{cases} \frac{1}{m(1+c)} \ln \left| \frac{mc+z/a}{mc-z/a} \right| + \frac{1}{z/a+m} \ln \left| \frac{mc-z/a}{(1+c)z/a} \right| \\ \quad + \frac{1}{z/a-m} \ln \left| \frac{mc+z/a}{(1+c)z/a} \right|, & z/a < -c \\ \frac{1}{2m(1+c)} \ln \frac{(m-1)(mc+z/a)}{(m+1)(mc-z/a)} + \frac{1}{2(z/a+m)} \ln \left| \frac{(m+1)(mc-z/a)}{(1+c)(1-z/a)z/a} \right| \\ \quad + \frac{1}{2(z/a-m)} \ln \left| \frac{(m-1)(mc+z/a)}{(1+c)(1-z/a)z/a} \right|, & -c < z/a < 0 \\ \frac{1}{2m(1+c)} \ln \frac{(m-1)(mc+z/a)}{(m+1)(mc-z/a)} + \frac{1}{2(z/a+m)} \ln \frac{(mc-z/a)(1+z/a)}{(m-1)(1+c)z/a} \\ \quad + \frac{1}{2(z/a-m)} \ln \frac{(mc+z/a)(1+z/a)}{(m+1)(1+c)z/a}, & 0 < z/a < c \\ 0, & z/a > c. \end{cases}$$

REFERENCES

Acreman, D.M., Stevens, I.R., Ponman, T.J. & Sakelliou, I. 2003, MNRAS, 341, 1333

Biller, B.A., Jones, C., Forman, W.R., Kraft, R. & Ensslin, T. 2004, ApJ, in press, astro-ph/0406132

Binney, J. & Tremaine, S. 1987, *Galactic Dynamics* (Princeton University Press, Princeton, NJ), p. 597

Bondi, H. 1952, MNRAS, 112, 195B

Brighenti, F. & Mathews, W.G. 1999, ApJ, 515, 542

Bullock, J.S., Kolatt, T.S., Sigad, Y., Somerville, R.S., Kravtsov, A.V., Klypin, A.A., Primack, J.R. & Dekel, A. 2001, MNRAS, 321, 559

Buote, D. 2002, ApJ, 574, L135

Buote, D. & Fabian, A. 1998, MNRAS, 296, 977

Burstein, D., Jones, C., Forman, W., Marston, A.P., & Marzke, R.O. 1997, ApJS, 111, 163

Byrd, G. & Valtonen, M. 1990, ApJ, 350, 89

Cecil, G., Gland-Hawthorn, J., & Veilleux, S. 2002, ApJ, 576, 745

Colbert, E.J.M. & Mushotzky, R.F. 1999, ApJ, 519, 89

Davis, D.S., Mulchaey, J.S., & Mushotzky, R.F. 1999, ApJ, 511, 34

Evrard, A.E., Metzler, C.A., & Navarro, J.F. 1996, ApJ, 469, 494

Fabbiano, G., Kim, D.W., & Trinchieri, G. 1992, ApJS, 80, 531

Forman, W., Schwarz, J., Jones, C., Liller, W., & Fabian, A. 1979, ApJ, 234, L27

Fujita, Y. 1998, ApJ, 509, 587

Garcia, A.M. 1993, A&AS, 100, 47

Gilfanov, M. 2004, MNRAS, 349, 146

Gilfanov, M., Grimm, H.-J. & Sunyaev, R. 2003, MNRAS, 339, 793

Gnedin, O.J. 2003, ApJ, 582, 141

Green, M.R., Godwin, J.G. & Peach, J.V. 1988, MNRAS, 234, 1051

Grimm, H.-J., Gilfanov, M., & Sunyaev, R. 2002, A & AS, 391, 923

Gunn, J., & Gott, J. 1972, ApJ, 176, 1

Heinz, S., Churazov, E., Forman, W.R., Jones, C. & Briel, V.G. 2003, MNRAS, 346, 13

Horellou, C. & Booth, R. 1997, A&AS, 126, 3

Horellou, C. & Koribalski 2003, Astrophys.& Space Sci., 284, 499

Hunt, R. 1971, MNRAS, 154, 141

Irwin, J.A. & Sarazin, C.L. 1996, ApJ, 471, 683

Jones, C., Stern, C., Forman, W., Breen, J., David, L., & Tucker, W. 1997, ApJ, 482, 143

Kannappan, S.J., Jansen, R.A. & Barton, E. J. 2004, AJ, 127, 1371

Kenney, J., et al. 1995, ApJ, 438, 135

Kenney, J., van Gorkom, J.H. & Vollmer, B. 2004, astro-ph/0403103

Landau, L.D. & Lifshitz, E.M. 1959, Fluid Mechanics (London:Pergamon), Chapter IX

Lauer, T., Gebhardt, K., Richstone, D., Tremaine, S., Bender, R., Bower, G., Dressler, A., Faber, S.M., Filippenko, A.V., Green, R., Grillmair, C., Ho, L.C., Kormendy, J., Magorrian, J., Pinkney, J., Laine, S., Postman, M., & van der Marel, R. 2002, AJ, 124, 1975

Lavery, R. & Henry, J.P. 1988, ApJ, 330, 596

Macchetto, F., Pastoriza, M., Caon, N., Sparks, W., Fravalisco, M., Bender, R., Capaccioli, M. 1996, A&AS, 120, 463

Machacek, M., Dosaj, A., Forman, W., Jones, C., Markevitch, M., Vikhlinin, A., Warmflash, A., & Kraft, R. 2004a, ApJ, submitted, eprint astro-ph/0408159

Markevitch, M., Mazzotta, P., Vikhlinin, A., Burke, D., Butt, Y., Donnelly, H., Forman, W.R., Harris, D., Kim, D.-W., Virani, S., & Vrtilek, J. 2003, ApJ, 586, L19

N. Martimbeau & J. Huchra, 2004, "CfA Redshift Catalog," on-line edition of October 2004, <http://cfa-www.harvard.edu/huchra/zcat>

Mihos, J.C., Bothun, G.D., & Richstone, D.O. 1993, ApJ, 418, 82

Moore, B., Katz, N., Lake, G., Dressler, A., & Oemler, A. 1996, Nature, 379, 613

Mulchaey, J.S., Davis, D.S., Mushotzky, R.F. & Burstein, D. 1996, ApJ, 456, 80

Mulchaey, J.S., Davis, D.S., Mushotzky, R.F. & Burstein, D. 2003, ApJS, 145, 39

Mulchaey, J.S. & Zabludoff, A.I. 1998, ApJ, 496, 73

Müller, M., Mair, G., & Hillebrandt, W. 1989, A&A, 216, 19

Navarro, J.F., Frenk, C.S., & White, S.D.M. 1995, MNRAS, 275, 56

Navarro, J.F., Frenk, C.S., & White, S.D.M. 1996, ApJ, 462, 563

Navarro, J.F., Frenk, C.S., & White, S.D.M. 1997, ApJ, 490, 493

Nulsen, P.J.E. 1982, MNRAS, 198, 1007

Osmond, J.P.F. & Ponman, T.J. 2004, MNRAS, 350, 1511

O'Sullivan, E., Forbes, D.A., & Ponman, T.J. 2001, MNRAS, 328, 461

Paolillo, M., Fabbiano, G., Peres, G. & Kim, D.-W. 2002, AJ, 565, 883

Pellegrini, S., Baldi, A., Fabbiano, G., & Kim, D.-W. 2003, ApJ, 597, 175

Pierce, M.J. & Tully, R.B. 1992, ApJ, 387, 47

Ponman, T., Bourner, P.D.J., Ebbling, H. & Böhringer 1996, MNRAS, 283, 690

Ptak, A., et al. 1999, ApJS, 120, 179

Quilis, V., Moore, B., & Bower, R. 2000, Science, 288, 1617

Rangarajan, F.V.N., Fabian, A.C., Forman, W.R. & Jones, C. 1995, MNRAS, 277, 1047

Read, A.M. & Ponman, T.J. 2003, A&A, 409, 395

Ruderman, M.A. & Spiegel, E.A. 1971, *ApJ*, 165, 1

Ruffert, M. 1994, *A&AS*, 106, 505

Sakelliou, I. 2000, *MNRAS*, 318, 1164

Sakelliou, I., Merrifield, M.R., & McHardy, I.M. 1996, *MNRAS*, 283, 673

Sarazin, C.L. 1988, *X-ray Emission from Clusters of Galaxies* (Cambridge University Press)

Scharf, C.A., Zurek, D.R., & Bureau, M. 2004, preprint astro-ph/0406216

Schulz, S. & Struck, C. 2001, *MNRAS*, 328, 185

Shapley, A., Fabbiano, G., & Eskridge, P.B. 2001, *ApJS*, 137, 139

Stevens, I.R., Acreman, D. & Ponman, T.J. 1999, *MNRAS*, 310, 663

Strickland, D., Heckman, T.M., Colbert, E.J.M., Hoopes, C.G. & Weaver, K.A. 2004 *ApJS*, 151, 193

Sun, M. & Vikhlinin, A. 2004, *ApJ*, submitted

Vikhlinin, A., Markevitch, M. & Murray, S.S. 2001, *ApJ*, 551, 160

Vollmer, B. 2003, *A&A*, 398, 525

Wang, Q.D., Owen, F., Ledlow, M., & Keel, W. 2004, in *Outskirts of Galaxy Clusters: Intense Life in the Suburbs*, Proceedings IAU Colloquium No. 195, ed. A. Diaferio, in press, preprint astro-ph/0404313

White, D., Fabian, A., Forman, W., Jones, C. & Stern, C. 1991, *ApJ*, 375, 35